Hochschule für Angewandte Wissenschaften Hamburg
Hamburg University of Applied Sciences

Masterarbeit

Methodische Untersuchungen zur numerischen Simulation der Kabinenakustik mit FEM

Vorgelegt von
Yi Qiao

vorgelegt am:	22. November. 2012
Erstprüfer:	Prof. Dr.-Ing. habil. Frank Ihlenburg
Zweitprüfer:	Dipl.-Ing Martin Wandel
Studiengang:	Berechnung und Simulation im Maschinenbau

Hochschule für Angewandte Wissenschaften Hamburg
Department Maschinenbau und Produktion, Fakultät TI

Abstract

It is very important to predict the acoustic behavior of the fuselage cabin for the noise control. Such coupled fluid-structure interaction problems can be solved by numerical simulation using finite element method. Following the reciprocity principle is introduced and tested on a simple model to verify the accuracy. Then a practical model of a fuselage cabin a is studied. On the basis of the sound pressure level results from each ear position of passengers, reciprocity principle and also other methods are employed for the peak frequencies to evaluate the structure parts that have most influence on the acoustic response. After that, the structure is improved base on the analysis results.

Key words: Cabin acoustics; Finite element method; Fluid-structure interaction; Reciprocity principle; Frequency response analysis; Acoustic contribution analysis.

Acknowledgements

First I would like to express my sincere gratitude to my supervisor Prof. Dr.-Ing. habil. Frank Ihlenburg. Without his patient guidance I could not have completed my thesis. And i wish to thank Dipl.-Ing Martin Wandel for providing this project and valuable advices. Besides, special thanks also to Berk Özer for proofreading the text. At last i would like to thank all my friends and my parents for their encouragement and support on my works.

Contents

List of Figures

List of Tables

List of Abbreviations

ABC Absorbing Boundary Conditions

DOF Degree of Freedom

ERP Equivalent Radiated Power

FEM Finite Element Method

FRA Frequency Response Analysis

FSI Fluid-Structure Interaction

PDE Partial Differential Equation

SEA Statistical Energy Analysis

SPL Sound Power Level

TMD Tuned Mass Damper

TPA Transfer Path Analysis

Chapter 1

Introduction

An important aspect in the development of new airplanes is acoustic comfort in both the passenger cabin and the crew workspace. In principle, predictions to vibro-acoustic behavior can be provided through numerical simulations referencing the virtual prototype. This master thesis aims to provide a numerical method based on finite elements analysis to improve the accuracy and efficiency of such predictions.

Figure 1.1: Cabin of airplanes [16]

1.1 Problem description

In the standard procedure, a new coupled calculation, which predicts the sound pressure at a particular reference point in the cabin over a frequency band by excited forces will be performed for each constructive variety. In this study, an alternative methodical approach, including both

calculation procedure and dependent parameter, will be tested. The optimization is based on the design process illustrated in figure 1.2.

1. The sound pressure level (SPL), or the frequency response function (FRF) at the desired location is evaluated for the original design.
2. According to the results, the structure components with significant influences will be determined at the peak frequencies.
3. On the basis of influential factors, modifications are made to improve the SPL.
4. The previous steps are iterated until the SPL requirement over the frequency range of interest is satisfied.

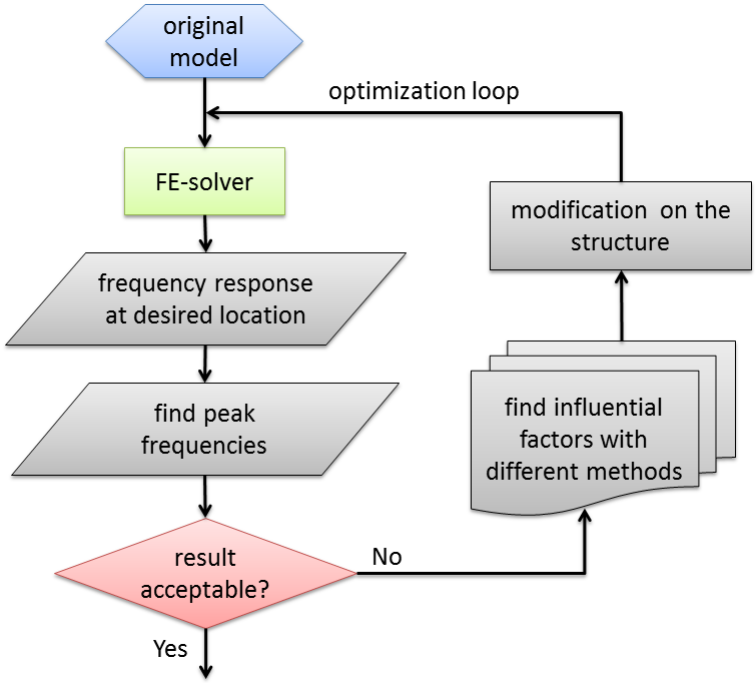

Figure 1.2: Flowchart of optimization process

This thesis mainly focuses on the evaluation methods and auxiliary goals used in the second and the third step to shorten the R&D cycle. Especially the following approaches and methods will be investigated:

- Vibro-acoustic transfer path analysis (TPA) calculation and the application of the reciprocity principle
- Calculation for acoustic or vibro-acoustic sound power and intensity

- Convenience from other auxiliary parameter such as modal participation, panel participation etc.

The analysis will first begin with simple models, and then, depending on the applicability, these methods will be scaled to the the real size of model.

1.2 Outline

The first chapter shortly introduces the goal of this investigation. Chapter 2 introduces fundamental principles, which are used in subsequent chapters and chapter 3 surveys existing methods and auxiliary quantities. Then, in chapter 4, these methods will be verified through basic-models. After that, in chapter 5 the methods are applied to the model of an airplane. Additionally, optimizations of the structure will be also estimated. And last chapter is conclusion of the work. The purpose of this chapter is to make an overview of and discuss the possible direction for the further development.

Chapter 2

Theory

This chapter summarizes the fundamental theories used as the basis for further discussion: The chapter begins with the fundamentals of acoustics, then the finite element method including fluid-structure interaction, and finally the reciprocity principle in vibro-acoustics will be explained.

2.1 Some basic foundations of acoustics

The physical state at every point of a fluid volume is characterized by three variables: Pressure, density and particle velocity

$$P(x,t) \quad \rho(x,t) \quad \mathbf{V}(x,t)$$

The state variables depend on each other. The governing equations of wave propagation can be formulated in terms of either pressure, density or particle velocity [1].

2.1.1 Sound pressure level

First and foremost, one shall get a clear idea about the task: What does "acoustic comfort" actually mean? It is known that sound is a mechanical wave that is an oscillation of pressure transmitted through an acoustic medium. These acoustic waves are essentially a type of longitudinal waves that propagate by means of compression and rarefaction as figure 2.1.

The compressions are regions of high pressure while the rarefactions are regions of low pressure. Based on the amplitude of the pressure one define the loudness of a tone as sound pressure level (dB) in logarithmic scale

$$p[dB] = 20 \log_{10} \frac{p[Pa]}{p_0[Pa]} \tag{2.1}$$

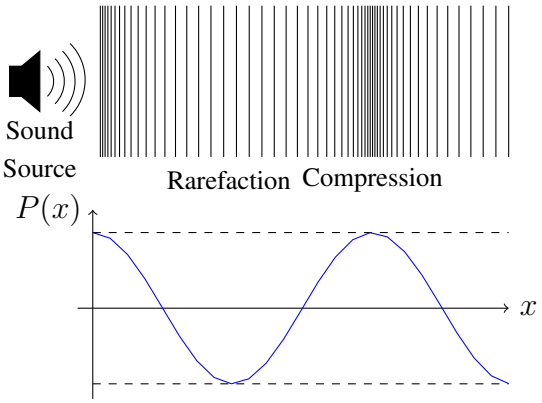

Figure 2.1: Rarefaction and compression of Sound wave

where the reference pressure $p_0 = 2.0 \times 10^{-5} Pa$.

The propagation of acoustic waves is detected by ears, where the audible hearing range is defined as the range of frequencies that can be heard by humans, generally between 20 Hz and 20 kHz. It is impractical and also unnecessary to investigate such a wide range. For industrial applications engineers are interested only in parts of the whole range, which is divided into several areas. The frequency range 20-200 Hz denotes the low frequency range.

Noise at low frequencies has a great impact on the acoustic quality. Low frequency noise has a totally different acoustical character than high frequency noise: High frequency noise attenuates rapidly with increasing distance or by barriers. Low frequency noise, however, is subject to less attenuation over a distance and can easily pass through barriers.

In the low frequency range, the finite elements method (FEM) and the boundary elements method (BEM) are widely used, while in the high frequency domain, where modal density is too high, the statistical energy analysis (SEA) is better suited. In this study, where we deal with low frequency noise produced by turbines, FEM is only employed to investigate sound propagation in the low frequency domain.

2.1.2 Wave equation and Helmholtz equation

Figure 2.2 shows a volume V that is being compressed under external pressure.

S is the surface of the volume and $\mathbf{n}$ is the unit normal vector of the boundary ∂V. The force along the boundary ∂V is then $\mathbf{F} = -\oint P\mathbf{n}dS$. Newton's second law $\mathbf{F} = m\mathbf{a}$ gives:

$$-\oint_{\partial V} P\mathbf{n}dS = \int_V \rho \frac{d\mathbf{V}}{dt} dV \tag{2.2}$$

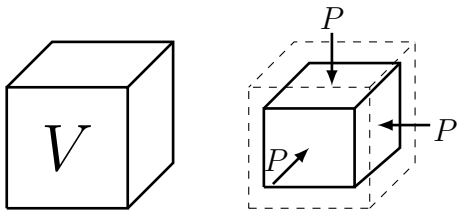

Figure 2.2: Compression of volume

The bulk modulus B of a material measures the resistance to uniform compression. It is defined as the ratio of the infinitesimal pressure increase to the resulting relative decrease of the volume V

$$P = -B\frac{dV}{V} \tag{2.3}$$

Using the relations $dV/V = div\mathbf{U}$ and $\mathbf{V} = \dot{\mathbf{U}}$, equation 2.2 and 2.3 can be combined to obtain the wave equation

$$\Delta p = \frac{1}{c^2}\ddot{P} \tag{2.4}$$

where Δ the Laplace operator, and the speed of sound is introduced by

$$c^2 = \frac{B}{\rho_0}$$

using further harmonic assumption

$$P(x,t) = p(x)e^{-i\omega t}$$

one gets the Helmholtz equation

$$\Delta p + k^2 p = 0 \tag{2.5}$$

where k is the wave number and depends on the frequency of the wave

$$k = \frac{\omega}{c}$$

The wave length of the acoustic wave is

$$\rho = \frac{2\pi}{k}$$

and hence

$$\rho = \frac{c}{f}$$

The Helmholtz equation provides the mathematical basis for sound propagation through fluids. Afterwards how to get the numerical solution becomes the central problem for computational acoustics.

2.1.3 Analytical solutions of the Helmholtz equation

The Helmholtz equation is a linear elliptic partial differential equation (PDE). The equation can be solved by separation of variables to reduce the complexity of the analysis [14]. Here Helmholtz problems will be illustrated in cartesian and spherical coordinates.

Cartesian coordinates

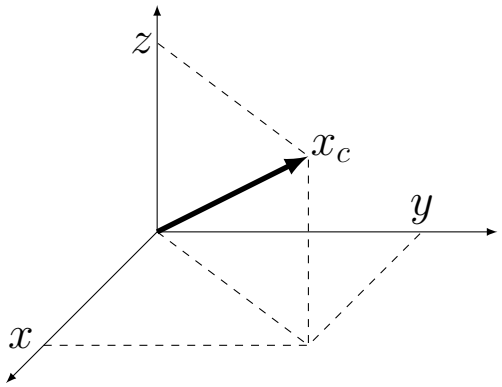

Figure 2.3: Illustration of the cartesian coordinate system

Consider the Helmholtz equation $\Delta p + k^2 p = 0$ in cartesian coordinates (figure 2.3). Since there are 3 dimensions, nontrivial solutions of the form $p(x, y, z) = X(x)Y(y)Z(z)$ are looked for:

$$X''YZ + XY''Z + XYZ'' + k^2XYZ = 0$$

Dividing each side by XYZ we obtain

$$\frac{X''}{X} + \frac{Y''}{Y} + \frac{Z''}{Z} + k^2 = 0$$

since each term in the equation depends on a different variable, all terms must be constant:

$$k_x^2 = -\frac{X''}{X}$$

$$k_y^2 = -\frac{Y''}{Y}$$

$$k_z^2 = -\frac{Z''}{Z}$$

After that the general form of plane waves is obtained:

$$p(\mathbf{x}) = e^{i\mathbf{kx}} \tag{2.6}$$

where wave vector $\mathbf{k}$ is satisfied the dispersion relation

$$|\mathbf{k}| = \sqrt{k_x^2 + k_y^2 + k_z^2}$$

Plane waves are important particular solutions of the 2-D and 3-D Helmholtz equations [2]. Arbitrary solutions of the wave equation can be expressed as a superposition of plane waves traveling into all possible directions in three-dimensional space.

Spherical coordinates

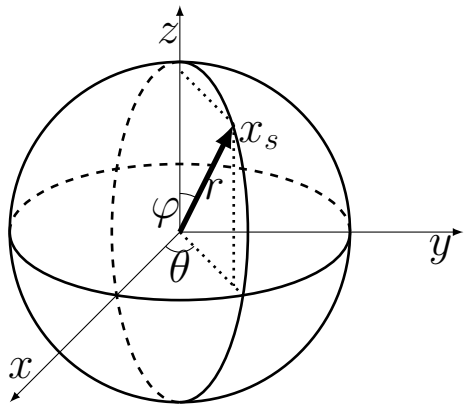

Figure 2.4: Illustration of the spherical coordinate system

In this section the solution for the exterior problem in spherical coordinates is presented, the coordinate system is shown in figure 2.4, one can transform the cartesian coordinates into spherical coordinates using following equations:

$$x = r\sin\theta\cos\phi$$

$$y = r\sin\theta\sin\phi$$

$$x = r\cos\theta$$

and again the separation of variables will be applied

$$p(r,\theta,\phi) = f(r)g(\theta)h(\phi)$$

leading to the separated ordinary differential equations (ODE)

$$\frac{d}{dr}\left(r^2\frac{df(r)}{dr}\right) + (k^2r^2 - \lambda)f(r) = 0 \tag{2.7}$$

$$\sin\theta\frac{d}{d\phi}\left(\sin\theta\frac{dg(\theta)}{d\theta}\right) + (\lambda\sin^2\theta - \nu)g(\theta) = 0 \tag{2.8}$$

$$\frac{d^2h(\phi)}{d\phi^2} + \nu h(\phi) = 0 \tag{2.9}$$

where λ and ν are constants. The function f is defined in the exterior of a sphere and the function g, h are defined on the surface S. Furthermore, the function f satisfies the Sommerfeld condition [2], which means that the sound waves are absorbed at infinity.

Through the derivation of the previous equations (2.7), (2.8), (2.9) one can obtain

$$p(r,\theta,\varphi) = \sum_{n=0}^{\infty} h_n(kr) \sum_{m=0}^{n} P_n^m(\cos\theta) \left(A_{mn}\cos(m\varphi) + B_{mn}\sin(m\varphi)\right) \tag{2.10}$$

where $h_n(kr)$ is the spherical Hankel functions and P_n^m denotes the Legendre polynomials.

This multipole expansion describes the radiation from bodies which are located at the origin and which are of finite extent can be characterized by sums of multipoles [5]. Another similar Atkinson-Wilcox expansion shows that any vector field satisfying the vector Helmholtz equation and the Silver-Mueller radiation condition can be expanded as a function of r [2]:

$$p(r) = \frac{e^{ikr}}{r} \sum_{n=0}^{\infty} \frac{A_n(\theta,\phi)}{r^n} \tag{2.11}$$

Moreover, multipoles are constructed from distributions of point sources. In case $n = 0$ the simplest multipole is received, the monopole

$$p(r) = \frac{A}{r} e^{ikr}, A \in \mathbb{C} \tag{2.12}$$

2.2 Vibroacoustic simulations with the finite element method

The finite element method (FEM) is a numerical method used for solving many practical engineering problems. In this study, the dynamic behavior will be predicted with FEM. One can begin with the equilibrium equations in dynamic analysis [3]

$$\mathbf{KU} + \mathbf{C}\dot{\mathbf{U}} + \mathbf{M}\ddot{\mathbf{U}} = \mathbf{F} \tag{2.13}$$

where $\mathbf{K}$ is the stiffness matrix, $\mathbf{C}$ is the damping matrix, $\mathbf{M}$ is the mass matrix, $\mathbf{F}$ is the external load vector, and $U\ \dot{U}\ \ddot{U}$ represent displacement, velocity and acceleration, respectively. There are two kinds of here to solve this equation. There are two ways to solve this equation: One can either use the direct solution or the modal solution.

2.2.1 Direct solution

As literally meaning direct solution solves this equation without any transformations. Assuming a time-harmonic excitation, and the response can be also written as

$$\mathbf{F} = \mathbf{f}e^{i\omega t} \quad \mathbf{U} = \mathbf{u}e^{i\omega t}$$

substitute them into equation (2.13) and get

$$\left[\mathbf{K} + i\omega\mathbf{C} - \omega^2\mathbf{M}\right]\mathbf{u} = \mathbf{f} \tag{2.14}$$

the term in square brackets is called dynamical stiffness matrix, then the inverse matrix of the dynamical stiffness matrix is computed

$$\mathbf{u} = \left[\mathbf{K} + \mathbf{i}\omega\mathbf{C} - \omega^{\mathbf{2}}\mathbf{M}\right]^{-1}\mathbf{f} \tag{2.15}$$

after that this matrix is multiplied with the load vector to obtain the direct solution. There are two advantages of the direct solution: It leads to the exact solution and is adequate for arbitrary damping. But one obvious disadvantage of direct solution is the time cost for calculation, since for each driving frequency the dynamic stiffness matrix must be recomputed and inverted [1]. For large models which contain millions of DOFs the modal solution may be advantageous.

2.2.2 Modal superposition

To get the modal superposition, the modal analysis is needed as the first step. Eigenvalues and eigenvectors of the undamped eigenproblem

$$\left[\mathbf{K} - \omega^2\mathbf{M}\right]\mathbf{x} = 0 \tag{2.16}$$

are computed and the eigenvectors $\mathbf{x_1}...\mathbf{x_N}(N \ll n)$ are grouped into a rectangular modal matrix. In the next step one assumes the displacement as the superposition from calculated eigenmodes

$$\mathbf{u} \approx \mathbf{u_N} = \mathbf{Xq} \tag{2.17}$$

where q denotes a weighting factor for each eignemode. The eigenmodes can be scaled such that the stiffness and mass matrices are decoupled as

$$\mathbf{X}^T\mathbf{K}\mathbf{X} = \boldsymbol{\omega}^2 = \begin{bmatrix} \omega_1^2 & & \\ & \ddots & \\ & & \omega_N^2 \end{bmatrix}_{N\times N} \tag{2.18}$$

$$\mathbf{X}^T\mathbf{M}\mathbf{X} = \mathbf{I} = \begin{bmatrix} 1 & & \\ & \ddots & \\ & & 1 \end{bmatrix}_{N\times N} \tag{2.19}$$

Substituting equation (2.17), (2.18), (2.19) into equation (2.14) gives

$$\left[\boldsymbol{\omega}^2 + i\omega\mathbf{X}^T\mathbf{C}\mathbf{X} - \omega^2\mathbf{I}\right]_{N\times N}\mathbf{q} = \mathbf{X}^T\mathbf{f} \tag{2.20}$$

If $\mathbf{X}^T\mathbf{C}\mathbf{X}$ is also diagonal,each component of the inverse equation after the system is decoupled, each component of this equation

$$\mathbf{q} = \left[\boldsymbol{\omega}^2 + i\omega\mathbf{X}^T\mathbf{C}\mathbf{X} - \omega^2\mathbf{I}\right]^{-1}\mathbf{X}^T\mathbf{f} \tag{2.21}$$

can be solved independently. Finally the back transformation is applied

$$\mathbf{u}_N = \mathbf{X}\mathbf{q} \tag{2.22}$$

to give the approximate solution. The main advantage of modal superposition is the lower computational effort due to the modal reduction and decoupling of equations. Hence the modal superposition is recommended for large matrix dimensions or large number of frequency steps.

2.2.3 Acoustic Simulations

For the purpose of the acoustic simulations, one usually applies 3-D elements with special fluid nodes.Normally, each node for solid elements in 3-D has 3 translational DOFs. The difference between solid nodes and fluid nodes is, for fluid nodes each node is associated with one DOF, namely the acoustic pressure. That is why it is said that the acoustic element is actually a simplified version of the solid element.

Furthermore, boundary conditions for fluid elements are totally different from common boundary conditions. Hence, special boundary conditions for the fluid element are needed in order to simulate some cases of acoustic problems such as free surfaces and rigid walls.

Here as an example one can recall the general solution of the 1-D Helmholtz equation

$$p(x) = C_1 e^{ikx} + C_2 e^{-ikx} \tag{2.23}$$

the first term on the righthand side represents an outgoing wave while the second term represent an incoming wave or reflected wave. Here the radiation conditions at the boundary is applied

$$\frac{dp}{dx} - ikp = 0 \tag{2.24}$$

to eliminate the incoming wave.

For a plane wave a non-reflecting boundary condition can be prescribed if its direction is known. In general, this is not possible. Instead, one can prescribe absorbing boundary conditions (ABC) as an approximation to non-reflecting conditions [2]. Equation 2.24 can be generalized to the impedance boundary condition. In mechanics, the stiffness of a structure at a certain point can be characterized by the relation of (complex) force amplitude to (complex) velocity amplitude.

The (complex) ratio f/v is called impedance. Carrying this notion over to acoustics, it can be written as

$$p' = ik\frac{Z_0}{Z_n}p \tag{2.25}$$

where the impedance Z_n denotes the ratio of the force amplitude to the particle velocity in the normal direction. The normal impedance for a plane wave is defined as

$$Z_n = \frac{P}{v_n} \tag{2.26}$$

and the characteristic impedance of the acoustic medium is equal to

$$Z_0 = \rho c \tag{2.27}$$

Special cases of the impedance boundary condition are summarized in the following table:

$Z_n = \infty$	$p' = 0$	**Complete Refection** (rigid boundary)
$Z_n = Z_0$	$p' = ikp$	**Complete Absorption** (radiation condition)
$Z_n = 0$	p=0	**Partial Reflection** (free end)

Table 2.1: Boundary conditions for different cases [1]

More details about the practical realization of such absorbing boundary conditions by FEM will be discussed later in chapter 5.

2.2.4 Fluid-structure interaction

Consider the boundary of the acoustic medium which is in contact with an elastic structure. The structure satisfies the dynamic equilibrium equations, and the fluid satisfies the wave equation. In order to establish the interaction between fluid and structure, two conditions are required at the boundaries. The first condition is the equilibrium on the coupling surface. For one point at the boundary, the normal projection of stress tensor is equal to the normal pressure from the fluid

$$\mathbf{t} = \boldsymbol{\sigma} \cdot \mathbf{n} = -P\mathbf{n} \tag{2.28}$$

Another condition is kinematic compatibility, which means the normal displacement of solid and fluid should be the same.

$$\mathbf{U}_s\mathbf{n} = \mathbf{U}_f\mathbf{n} \tag{2.29}$$

Since friction is neglected, no condition can be imposed on the tangential projections of the displacement vectors [1]. The fluid displacement vector can be replaced by the pressure value using the Euler equation in the fluid

$$\rho_0 \ddot{\mathbf{U}}_s \cdot \mathbf{n} = -\nabla P \cdot \mathbf{n} \tag{2.30}$$

The discretized dynamic equation of motion for the structure can be written as

$$\mathbf{K_s U} + \mathbf{C_s}\dot{\mathbf{U}} + \mathbf{M_s}\ddot{\mathbf{U}} = \mathbf{F_s} \tag{2.31}$$

Similarly, the dynamic equation of motion for the fluid is

$$\mathbf{K_f P} + \mathbf{C_f}\dot{\mathbf{P}} + \mathbf{M_f}\ddot{\mathbf{P}} = \mathbf{F_f} \tag{2.32}$$

Applying the coupling equation 2.28 and 2.30 to the weak formulation of the structural and fluid differential equations, the distretized coupled system is obtained in the form

$$\begin{bmatrix} \mathbf{K}_s & \mathbf{A}_{sf} \\ 0 & \mathbf{K}_f \end{bmatrix} \begin{Bmatrix} \mathbf{U} \\ \mathbf{P} \end{Bmatrix} + \begin{bmatrix} \mathbf{C}_s & 0 \\ 0 & \mathbf{C}_f \end{bmatrix} \begin{Bmatrix} \dot{\mathbf{U}} \\ \dot{\mathbf{P}} \end{Bmatrix} + \begin{bmatrix} \mathbf{M}_s & 0 \\ -\mathbf{A}_{fs} & \mathbf{M}_f \end{bmatrix} \begin{Bmatrix} \ddot{\mathbf{U}} \\ \ddot{\mathbf{P}} \end{Bmatrix} = \begin{Bmatrix} \mathbf{F}_s \\ \mathbf{F}_f \end{Bmatrix} \tag{2.33}$$

where the coupling matrix $\mathbf{A}_{sf}$ $\mathbf{A}_{fs}$ contains the relations between structural and fluid nodes on the coupling surfaces. The equations can be scaled such that $\mathbf{A}_{sf} = \mathbf{A}_{fs}^T = \mathbf{A}$. If one derives the structural system once in the time variable and solves for the structural velocity instead of structural displacements, the coupling matrices are included into the global damping matrix viz[4]

$$\begin{bmatrix} \mathbf{K}_s & 0 \\ 0 & \mathbf{K}_f \end{bmatrix} \begin{Bmatrix} \mathbf{V} \\ \mathbf{P} \end{Bmatrix} + \begin{bmatrix} \mathbf{C}_s & \mathbf{A} \\ -\mathbf{A}^T & \mathbf{C}_f \end{bmatrix} \begin{Bmatrix} \dot{\mathbf{V}} \\ \dot{\mathbf{P}} \end{Bmatrix} + \begin{bmatrix} \mathbf{M}_s & 0 \\ 0 & \mathbf{M}_f \end{bmatrix} \begin{Bmatrix} \ddot{\mathbf{V}} \\ \ddot{\mathbf{P}} \end{Bmatrix} = \begin{Bmatrix} \dot{\mathbf{F}}_s \\ \mathbf{F}_f \end{Bmatrix} \tag{2.34}$$

If the forcing terms are time-harmonic with a forcing frequency ω, one can obtain the symmetrical coupled system of linear stationary nodal equations

$$\left(\begin{bmatrix} \mathbf{K}_s & 0 \\ 0 & -\mathbf{K}_f \end{bmatrix} + i\omega \begin{bmatrix} \mathbf{C}_s & \mathbf{A} \\ \mathbf{A}^T & -\mathbf{C}_f \end{bmatrix} - \omega^2 \begin{bmatrix} \mathbf{M}_s & 0 \\ 0 & -\mathbf{M}_f \end{bmatrix} \right) \begin{Bmatrix} \mathbf{v} \\ \mathbf{p} \end{Bmatrix} = \begin{Bmatrix} i\omega \mathbf{f}_s \\ -\mathbf{f}_f \end{Bmatrix} \tag{2.35}$$

After finite element matrices are assembled, the system of complex linear equations can be solved by calculating the inverse matrix for each forcing frequency ω. This is called the direct method.

Another option is modal superposition, setting

$$\mathbf{v} \approx \Phi_s \xi_s \qquad \mathbf{p} \approx \Phi_f \xi_f \tag{2.36}$$

the method is similar to the on which introduced in section 2.2.2. Note that the uncoupled eigenmodes for both structure and fluid separately are employed. Here the vectors ξ_s and ξ_f are

complex-valued modal coefficients; Φ_s are the uncoupled, undamped structural modes and Φ_f are the uncoupled, undamped, rigid-wall acoustic modes. Generally one only pays attention to the lower N eigenvectors, hence Φ_s and Φ_f usually have a reduced size of $N \times n$, depending on how many eigenvectors are chosen. Substituting this assumption into equation 2.35 and multiplying from the left by Φ_s^T and Φ_f^T leads to

$$\begin{aligned}\Big(\begin{bmatrix} \mathbf{\Phi}_s^T \mathbf{K}_s \mathbf{\Phi}_s & 0 \\ 0 & -\mathbf{\Phi}_f^T \mathbf{K}_f \mathbf{\Phi}_f \end{bmatrix} - i\omega \begin{bmatrix} \mathbf{\Phi}_s^T \mathbf{C}_s \mathbf{\Phi}_s & \mathbf{\Phi}_s^T \mathbf{A} \mathbf{\Phi}_f \\ \mathbf{\Phi}_f^T \mathbf{A}^T \mathbf{\Phi}_s & -\mathbf{\Phi}_f^T \mathbf{C}_f \mathbf{\Phi}_f \end{bmatrix} \\ -\omega^2 \begin{bmatrix} \mathbf{\Phi}_s^T \mathbf{M}_s \mathbf{\Phi}_s & 0 \\ 0 & -\mathbf{\Phi}_f^T \mathbf{M}_f \mathbf{\Phi}_f \end{bmatrix} \Big) \begin{Bmatrix} \xi_s \\ \xi_f \end{Bmatrix} = \begin{Bmatrix} -i\omega \mathbf{\Phi}_s^T \mathbf{f}_s \\ -\mathbf{\Phi}_f^T \mathbf{f}_f \end{Bmatrix}\end{aligned} \tag{2.37}$$

This modal equation can be solved to obtain the modal coefficients ξ_s and ξ_f. After that through back-transform (equation 2.36) the response is received for both structure and fluid respectively.

2.3 Reciprocity principle in vibro-acoustics

The reciprocity principle is widely used in many fields especially in vibro-acoustics. For example reciprocity principle allows a more convenient placement of the sound pressure sensor by the measurement in some special cases. Moreover the time cost of the simulation can be also improved by using this principle. And the theoretical background of reciprocity principle will be explained in the following sections.

2.3.1 Maxwell-Betti reciprocal work theorem

One shall begin with the most basic static case: Consider a elastic beam with an external force (shown in figure 2.5), the work done by these forces will transform into the elastic energy.
First assume a vertical force acting on the point A, and it produce a displacement in the same place ΔAA. Hence the work can be written as below:

$$W_A = \frac{1}{2} F_A \Delta AA$$

Second step another force is applied on the point B, the beam has a further displacement and an additional work

$$W_B = \frac{1}{2} F_B \Delta BB + F_A \Delta AB$$

thus the total work is

$$W_1 = W_A + W_B = \frac{1}{2} F_A \Delta AA + \frac{1}{2} F_B \Delta BB + F_A \Delta AB$$

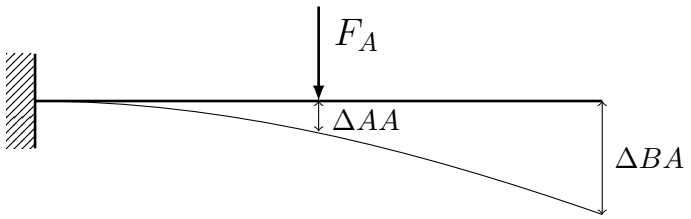

(a) first step: apply force F_A at point A

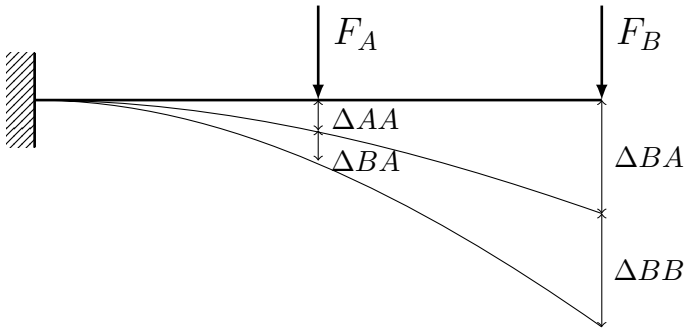

(b) second step: apply force F_B at point B

Figure 2.5: Maxwell-Betti reciprocal work theorem

Let us now consider another possibility and name it case 2: The force F_B is first applied and F_A afterwards. The total work is similarly

$$W_2 = \frac{1}{2}F_B\Delta BB + \frac{1}{2}F_A\Delta AA + F_B\Delta BA$$

Obviously, the total work will not be influenced by reversing the order of the loads i.e. $W_1 = W_2$, and through the elimination on both sides one can finally receive

$$F_A\Delta AB = F_B\Delta BA \tag{2.38}$$

which means if $F_A = F_B$, the displacement at point B caused by F_A is exactly the same as the displacement at point A caused by F_B. The Maxwell-Betti reciprocal work theorem can be also applied for other degrees of freedoms such as rotations and torques. Moreover, a similar relation still hold true for dynamic cases, this will be explained in the next section.

2.3.2 Vibrational reciprocity

It was Lord Rayleigh who first presented the general theory of vibrational reciprocity as applied to passive linear, distributed elastic systems having time-invariant physical parameters. Fahy demonstrated the vibrational reciprocity in his work [8]. Consider such a system, whose position is specified by a finite number of independent coordinates $\psi_1, \psi_2, \psi_3, etc.$ With an arbitrary small displacement the potential energy V can be described as a homogeneous quadratic

function of the coordinates

$$V = \frac{1}{2}c_{11}\psi_1^2 + \frac{1}{2}c_{22}\psi_2^2 + \cdots + c_{12}\psi_1\psi_2 + c_{23}\psi_2\psi_3 \ldots \tag{2.39}$$

and the kinetic energy T as a homogeneous quadratic function of coordinate velocities

$$T = \frac{1}{2}a_{11}\dot{\psi}_1^2 + \frac{1}{2}a_{22}\dot{\psi}_2^2 + \cdots + a_{12}\dot{\psi}_1\dot{\psi}_2 + a_{23}\dot{\psi}_2\dot{\psi}_3 \ldots \tag{2.40}$$

Lagrangian function, which denotes the dynamics of the entire system, is derived from these two energy functions $L = T - V$, substitute it into the Euler-Lagrange equations

$$\frac{d}{dt}\left(\frac{\partial L}{\partial \dot{\psi}}\right) - \frac{L}{\dot{\psi}} = 0 \tag{2.41}$$

and receive

$$\frac{d}{dt}\left(\frac{\partial T}{\partial \dot{\psi}}\right) - \frac{\partial T}{\partial \psi} + \frac{\partial V}{\partial \psi} = \Psi \tag{2.42}$$

where Ψ are the forces acting on the system that are not associated with the potential energy V. Furthermore there is also another group of forces which is caused by friction or viscosity. If one suppose each particle of the system is retarded by forces proportional to its component velocities, these forces can be formulated as the dissipation function

$$F = \frac{1}{2}b_{11}\dot{\psi}_1^2 + \frac{1}{2}b_{22}\dot{\psi}_2^2 + \cdots + b_{12}\dot{\psi}_1\dot{\psi}_2 + b_{23}\dot{\psi}_2\dot{\psi}_3 \ldots \tag{2.43}$$

After separating the dissipative forces from the term Ψ, one receives equations of motion of the form

$$\frac{d}{dt}\left(\frac{\partial T}{\partial \dot{\psi}}\right) - \frac{\partial T}{\partial \psi} + \frac{\partial F}{\partial \dot{\psi}} + \frac{\partial V}{\partial \psi} = \Psi \tag{2.44}$$

Substituting the three functions T, V, F into Lagrange's equation yields the following system of equations:

$$\begin{aligned} \overline{11}\psi_1 + \overline{12}\psi_2 + \overline{13}\psi_3 + \cdots &= \Psi_1, \\ \overline{21}\psi_1 + \overline{22}\psi_2 + \overline{23}\psi_3 + \cdots &= \Psi_2, \\ \overline{31}\psi_1 + \overline{32}\psi_2 + \overline{33}\psi_3 + \cdots &= \Psi_3, \end{aligned} \tag{2.45}$$

where each coefficient $\overline{rs}$ is an abbreviation for the quadratic operator, thus $\overline{rs}$ is equivalent to $(a_{rs}) + (b_{rs}) + (c_{rs})$. Since all these quantities $a_{rs}\ b_{rs}\ c_{rs}$ are constant and

$$a_{rs} = a_{sr} \quad b_{rs} = b_{sr} \quad c_{rs} = c_{sr}$$

the operations exhibit an important property

$$\overline{rs} = \overline{sr} \tag{2.46}$$

Which means, if a point harmonic force is applied to one coordinate and the oscillatory displacement is observed at another, solutions of the equations of motion show that the complex

ratio of displacement to force is invariant with respect to exchange of input and output coordinates. Rayleigh has demonstrated in his paper applications in which forces and couples, as well as translational and rotational displacements, are involved. These examples are illustrated in figure. 2.6 [8].

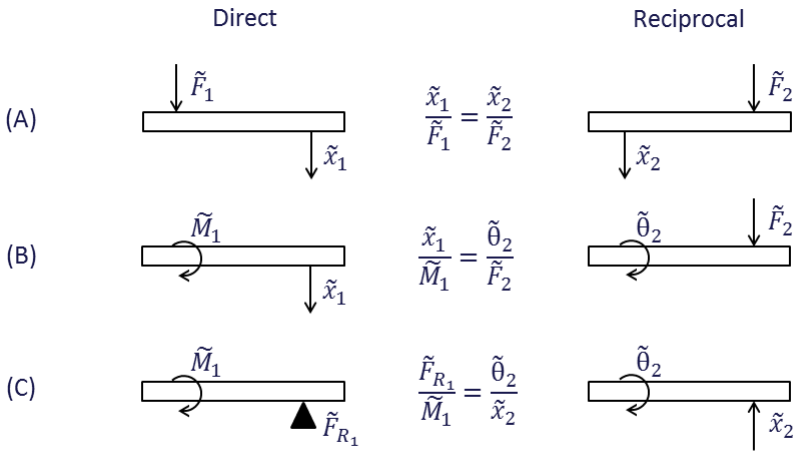

Figure 2.6: Various realizations of Rayleigh's reciprocity principle

2.3.3 Acoustic Reciprocity

A homogeneous fluid at rest behaves like a linear elastic medium in response to small applied disturbances and therefore obeys Rayleigh's vibrational reciprocity principle. In air, energy dissipation arises from viscothermal and molecular relaxation mechanisms; but, in cases of practical interest in the field of vibroacoustics, dissipative effects are weak, and reciprocity is found to apply provided that nonlinear sound propagation is avoided (sound pressure level less than about 130 dB in air)[8]. To derive the reciprocity principle in acoustic cases, the acoustic sound sources should be first introduced. As the fundamental acoustic source, monopoles are often used, which is described by its volume velocity

$$Q = \int_S v_n dA \quad \left[\frac{m^3}{s}\right] \tag{2.47}$$

and it can be shown as following figure where S is the surface of a sphere surrounding the source and $v_n = v \cdot \mathbf{n}$ is the normal projection of the complex sound velocity amplitude in the acoustic medium. Such point source corresponds to the case where the radius of the sphere is very small compared to the acoustic wavelength $ka \ll 1$. According to the definition the source strength $Q = S \cdot v_n = 4\pi a^2 v_n$, then the solution of the field is obtained

$$p(r) = -\frac{e^{ikr}}{4\pi r} \tag{2.48}$$

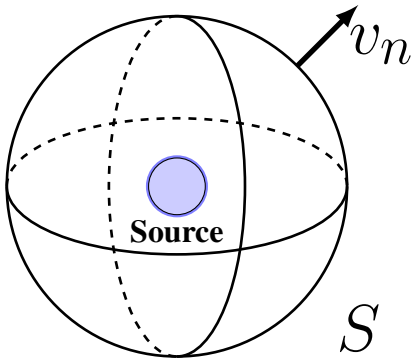

Figure 2.7: Source strength

In the next step it is employed in the inhomogeneous Helmholtz equation, let $p^{(1)}$ be the field caused by a point source at $\mathbf{r}_1$ with source strength $Q^{(1)}$ and use Green's function

$$\Delta p^{(1)} + k^2 p^{(1)} = -Q^{(1)}\delta(\mathbf{r} - \mathbf{r}_1) \tag{2.49}$$

Similarly, let $p^{(2)}$ be another field caused by a point source at $\mathbf{r}_2$

$$\Delta p^{(2)} + k^2 p^{(2)} = -Q^{(2)}\delta(\mathbf{r} - \mathbf{r}_2) \tag{2.50}$$

where superscript $(1), (2)$ means different fields. After that, one shall multiply equation 2.49 by $p^{(2)}$ and 2.49 by $p^{(1)}$and add them together

$$p^{(2)}\Delta p^{(1)} - p^{(1)}\Delta p^{(2)} = p^{(1)}Q^{(2)}\delta(\mathbf{r} - \mathbf{r}_2) - p^{(2)}Q^{(1)}\delta(\mathbf{r} - \mathbf{r}_1) \tag{2.51}$$

integrate both sides of equation 2.50. Since the left-hand side is equal to zero, one receives

$$\frac{\widetilde{p}_1}{\widetilde{Q}_1} = \frac{\widetilde{p}_2}{\widetilde{Q}_2} \tag{2.52}$$

This equation means the ratio between pressure amplitude and source strength remains constant, even if the position of source and microphone are interchanged.

2.3.4 Lyamshev Reciprocity

In 1959 Lyamshev demonstrated that linear elastic structures that are contiguous with a fluid may be incorporated into the total dynamic system to which reciprocity applies [9]. Let an arbitrary volume Ω be filled with the combination of acoustic media and a closed elastic envelopes, whose surface is marked as S_i, and it has a fixed contour by Γ_i (figure 2.8). Consider a field $p^{(1)}(\mathbf{r})$ caused by harmonic source $Q^{(1)}(\mathbf{r})$, which is continuously distributed in volume Ω

$$\triangle p^{(1)}(\mathbf{r}) + k^2 p^{(1)}(\mathbf{r}) = -Q^{(1)}(\mathbf{r}) \tag{2.53}$$

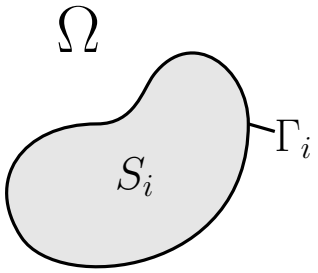

Figure 2.8: Sketch of the whole volume Ω

and satisfies the following boundary conditions

$$\lim_{\mathbf{r}\to\infty} p^{(1)}(\mathbf{r}) \to 0, \quad Imk > 0 \tag{2.54}$$

$$-\frac{1}{\omega^2\rho}\frac{\partial p^{(1)}(\mathbf{r})}{\partial n}\Big|_{S_i} = \omega_i^{(1)}(\mathbf{r}) \tag{2.55}$$

$$L_i\omega_i^{(1)}(\mathbf{r}) = F_i^{(1)}(\mathbf{r}) - p^{(1)}(\mathbf{r})\,\big|_{S_i} \tag{2.56}$$

$$T_{ij}(\omega_i^{(1)}) = g_{ij}^{(1)}\,\big|_{\Gamma_i'}, \quad R_{ij}(\omega_i^{(1)}) = -f_{ij}^{(1)}\,\big|_{\Gamma_i''}, \quad \Gamma_i' + \Gamma_i'' = \Gamma_i \tag{2.57}$$

in the above expressions

$\underline{n}$ is the external normal to S_i

ω_i is the normal displacement of the surface of the envelope

F_i is the external mechanical force

g_{ij}, f_{ij} are external loads acting along the contour Γ_i

$L_i\omega_i$ is a self-adjoint differential operator

Let $Q^{(2)}(r)$ be another given system of continuously distributed sources. Then the field $p^{(2)}(r)$ is obtained in a similar form

$$\Delta p^{(2)}(\mathbf{r}) + k^2 p^{(2)}(\mathbf{r}) = -Q^{(2)}(\mathbf{r}) \tag{2.58}$$

with similar boundary conditions as in equation 2.53. One can multiply equation 2.53 by $p^{(2)}(\mathbf{r})$ and equation 2.58 by $p^{(1)}(\mathbf{r})$, add them, and integrate both sides of the equation obtained through

the volume Ω. Using Green's formula, the boundary conditions 2.54 - 2.57, finally one obtains

$$\int_{\Omega} Q^{(2)}(\mathbf{r})p^{(1)}(\mathbf{r})dv + \sum_{i=1}^{k}\int_{S_i}\frac{\partial p^{(1)}(\mathbf{r})}{\partial n}F_i^{(2)}(\mathbf{r})ds + \sum_{i=1}^{m}\int_{\Gamma'}\sum_{j=1}^{N} g_{ij}^{(2)}R_{ij}\left(\frac{\partial p^{(1)}}{\partial n}\right)dl$$
$$+\sum_{i=1}^{m}\int_{\Gamma''}\sum_{j=1}^{N} f_{ij}^{(2)}T_{ij}\left(\frac{\partial p^{(1)}}{\partial n}\right)dl = \int_{\Omega} Q^{(1)}(\mathbf{r})p^{(2)}(\mathbf{r})dv + \sum_{i=1}^{k}\int_{S_i}\frac{\partial p^{(2)}(\mathbf{r})}{\partial n}F_i^{(1)}(\mathbf{r})ds \tag{2.59}$$
$$+\sum_{i=1}^{m}\int_{\Gamma'}\sum_{j=1}^{N} g_{ij}^{(1)}R_{ij}\left(\frac{\partial p^{(2)}}{\partial n}\right)dl + \sum_{i=1}^{m}\int_{\Gamma''}\sum_{j=1}^{N} f_{ij}^{(1)}T_{ij}\left(\frac{\partial p^{(2)}}{\partial n}\right)dl$$

equation 2.59 can be considered as a mathematical formulation of the acoustic principle of reciprocity. In some special cases, if

$$F_i^{(1)} = F_i^{(2)} = g_{ij}^{(1)} = g_{ij}^{(2)} = f_{ij}^{(1)} = f_{ij}^{(2)} = 0 i = 1, 2, \ldots, k; j = 1, 2, \ldots, N.$$

which means there is no external loads applied on the envelope, therefore only 2 terms remain exist

$$\int_{\Omega} Q^{(1)}(\mathbf{r})p^{(2)}(\mathbf{r})dv = \int_{\Omega} Q^{(2)}(\mathbf{r})p^{(1)}(\mathbf{r})dv \tag{2.60}$$

this relation is similar with the equation, which is proved in section 2.3.2. If the following conditions are assumed

$$Q^{(2)}(\mathbf{r}) = F_i^{(1)}(\mathbf{r}) = g_{ij}^{(1)} = g_{ij}^{(2)} = f_{ij}^{(1)} = f_{ij}^{(2)} = 0, i = 1, 2, \ldots, k; j = 1, 2, \ldots, N;$$
$$F_i^{(2)} = 0, i = 2, 3, \ldots, k.$$

then one gets

$$\int_{\Omega} Q^{(1)}(\mathbf{r})p^{(2)}(\mathbf{r})dv = \int_{S}\frac{\partial p^{(1)}(\mathbf{r})}{\partial n}F^{(2)}(\mathbf{r})ds \tag{2.61}$$

and it can be written in a simplified form

$$\frac{\widetilde{P}}{\widetilde{F}} = \frac{\widetilde{v}}{\widetilde{Q}} \tag{2.62}$$

An important practical consequence of this conclusion is that the transfer function betweens a mechanical vibrational force applied to an elastic plate or shell and the resulting sound pressure in a contiguous fluid may be determined by insonifying a structure by means of an omnidirectional "point" source, as illustrated in Fig. 2.9

2.3.5 Reciprocity for FE models

For FE models the reciprocity principle can be represented as transfer function, which describes the linear relation between input and output of a system. For structure case, the transfer function can be written as

$$u_i = h_{ij} f_j$$

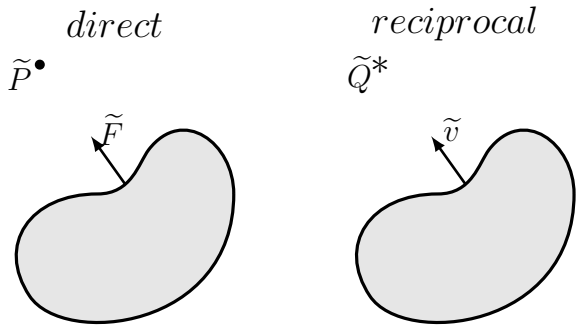

Figure 2.9: Lyamshev reciprocity relation for elastic structures excited by point forces

each value of h_{ij} means the response at degree of freedom i caused by a unit excitation at degree of freedom j. If the system contains n DOFs, then the complete transfer function should be a $n \times n$ matrix, and it actually the same as the inverse matrix of the dynamical stiffness matrix

$$\mathbf{U} = \mathbf{HF} = (\mathbf{K} + i\omega\mathbf{C} - \omega^2\mathbf{M})^{-1}\mathbf{F}$$

where the stiffness matrix

$$\mathbf{K} = \int_V \mathbf{B}^T\mathbf{E}\mathbf{B}dV$$

matrix $\mathbf{B}$ is made up of differential operator $\mathbf{D}$ and shape function $\mathbf{N}$

$$\mathbf{B} = \mathbf{DN}$$

and mass matrix

$$\mathbf{M} = \int_V \mathbf{N}^T\mathbf{N}dV$$

Furthermore, the damping matrix $\mathbf{C}$ in Rayleigh damping is defined proportional to the stiffness and mass matrix base on the damping coefficient. Since all components of the dynamical stiffness matrix can be proved to be symmetric, then the inverse matrix of a it, namely transfer matrix is also symmetric. Thus one can get this useful property of transfer matrix

$$h_{ij} = h_{ji} \tag{2.63}$$

additionally, for FSI cases the transfer matrix will be

$$\begin{bmatrix} \mathbf{V} \\ \mathbf{P} \end{bmatrix} = \begin{bmatrix} \mathbf{F} \\ \mathbf{Q} \end{bmatrix} \begin{bmatrix} \mathbf{H}_{ss} & \mathbf{H}_{sf} \\ \mathbf{H}_{fs} & \mathbf{H}_{ff} \end{bmatrix} \tag{2.64}$$

Because the coupling matrix is also symmetric, the reciprocity principle still holds true.

Chapter 3

Methods for evaluating influential components

The target of this study is a better acoustic comfort performance, hence referring to some methods is necessary to reach our goal. In an airplane, noise is mostly generated by the turbine in either vibration or noise form, transmitted through structure paths, and then radiated acoustically into the cabin. This is classified as ”structure-borne” noise. The transfer path is shown in following figure:

Figure 3.1: Process of propagation of noise

Obviously, the transfer path features prominently in the whole process. The noise will be either isolated or amplified, depending on the sensitivity of the transfer path. There are some auxiliary functions can be interpreted as intermediate index on the transfer path from noise source to receiver. These methods and auxiliary parameters like ERP, Modal/Panel Participation quantities are introduced in this chapter.

3.1 Modal Participation & Panel Participation

Reduce the noise level in the cabin is a quite common problem in the industrial field such as automobile manufacturers. For this reason frequency response analysis (FRA) is routinely applied

to predict the dynamic behavior under vibrational excitation especially the resonant frequencies. However, knowing the location of the resonant peaks is not enough. In order to modify the system effectively, modal/panel participation factor can be used to investigate further about these resonant frequencies.

In an acoustic analysis, the pressure at a grid point is considered the sum of the pressures due to the responses of the different fluid modes. Recall the fluid and structure equations of motion for a coupled system with time-harmonic excitation [6]

$$\left(\begin{bmatrix} \hat{\mathbf{K}}_s & \hat{\mathbf{A}} \\ 0 & \hat{\mathbf{K}}_f \end{bmatrix} + i\omega \begin{bmatrix} \hat{\mathbf{C}}_s & 0 \\ 0 & \hat{\mathbf{C}}_f \end{bmatrix} - \omega^2 \begin{bmatrix} \hat{\mathbf{M}}_s & 0 \\ -\hat{\mathbf{A}}^T & \hat{\mathbf{M}}_f \end{bmatrix} \right) \begin{Bmatrix} \xi_s \\ \xi_f \end{Bmatrix} = \begin{Bmatrix} \hat{\mathbf{F}}_s \\ \hat{\mathbf{F}}_f \end{Bmatrix} \tag{3.1}$$

where the hat denotes the modal transforms such as $\hat{K}_s = \Phi_s^T K_s \Phi_s, \hat{F}_s = \Phi_s^T K_s$.
For the bottom part of equation 3.1

$$\omega^2 \hat{A}^T \xi_s + (-\omega^2 \hat{M}_f + i\omega \hat{C}_f + \hat{K}_f)\xi_f = \hat{F}_f \tag{3.2}$$

Here one can define

$$Z = (-\omega^2 \hat{M}_f + i\omega \hat{C}_f + \hat{K}_f)^{-1} \tag{3.3}$$

then

$$\xi_f = -\omega^2 Z \hat{A}^T \xi_s + Z \hat{F}_f \tag{3.4}$$

The fluid mode participation is defined as

$$P_f = \Phi_f \xi_f \tag{3.5}$$

where ξ_f is the diagonalized vector of fluid modal amplitudes per excitation frequency ω. Acoustic fluid modal participation factor allows to identify the fluid modes that have the largest influence on the response. However, modal participation factor, by their nature, is useful only in the low-frequency range where the resonance frequencies are well separated, and the response is dominated by a small number of modes. On the contrary, geometric participation factor is useful also at higher frequencies where the response has contributions from a large number of modes [6]. There are two types of geometric participation factors, namely panel participation factor and grid participation factor. In this study only panel participation factor is used.

A panel is a set of grid points of the wetted surface. The panel participation factor is that pressure at the grid point considered that results from the accelerations of the grid points of the panel only, with all other grid points of the wetted surface kept fixed [6]. The wetted surface is divided into n subdomains, and the coupling matrix is made up of these subdomaians

$$A = A_1 + A_2 + \cdots + A_n \tag{3.6}$$

for each panel, the fluid-structure panel participation is defined as

$$P_p = -\omega^2 \Phi_f Z \Phi_f^T A_{panel}^T \Phi_s \xi_s \tag{3.7}$$

Thus, panel participation factor allows to identify the regions of the wetted surface that have the largest influence on the acoustic pressure at the grid point considered. In that case, when the panels do not overlap and their union equals the complete wetted surface. Then all the panel participation factor can be summed up to the total acoustic pressure.

3.2 Sound power

One common property of different sorts of noise is, that, they are all oscillatory waves and essentially a kind of propagation of energy. In many practical engineering applications the noise radiated from a structure, namely sound power or acoustic power is a significant auxiliary parameters and sometimes concerns the response of the system mostly. Thus, it is important to identify those parts of the structure which contribute most and to identify those frequencies where the radiation becomes maximal.

Assuming an arbitrary fluid particle in the field, and its total energy is composed of kinetic energy and potential energy

$$E = E_{kin} + E_{pot} = \frac{1}{2}\rho_0 |\mathbf{V}|^2 + \frac{1}{2}\frac{P^2}{B} \tag{3.8}$$

Sound intensity is defined as the sound power P per unit area A

$$\frac{\partial E}{\partial t} = -\mathrm{div}\mathbf{I} \tag{3.9}$$

From equation 3.8, the time derivation of energy is

$$-\frac{\partial E}{\partial t} = -\rho_0 \mathbf{V} \cdot \frac{\partial \mathbf{V}}{\partial t} - \frac{P}{\rho_0 c^2}\frac{\partial P}{\partial t} = \bigtriangledown P \cdot \mathbf{V} + P\mathrm{div}\mathbf{V} = \mathrm{div}(P\mathbf{V}) \tag{3.10}$$

Hence the acoustic intensity is equal to the product of the real parts of the instantaneous pressure and the velocity at the point

$$\mathbf{I} = P\mathbf{V} \tag{3.11}$$

If pressure and velocity are time-harmonic, then both real part can be computed by

$$\begin{aligned} (\mathrm{Re}P)(\mathrm{Re}V) &= \frac{1}{2}[\mathrm{Re}(PV) + \mathrm{Re}(PV^*)] \\ &= \frac{1}{2}[\mathrm{Re}(pv)\cos 2\omega t - \mathrm{Im}(pv)\sin 2\omega t + \mathrm{Re}(pv^*)] \end{aligned} \tag{3.12}$$

since the time-average of the first two terms vanish, one obtains

$$\langle \mathbf{I} \rangle = \frac{1}{2} p \mathbf{v}^* \tag{3.13}$$

where p is pressure and v^* is the complex conjugate of velocity. The integral of the sound intensity over the entire surface provides the radiated sound power

$$\mathsf{P} = \iint \mathbf{I} d\mathbf{A} = \frac{1}{2} \mathbb{R} \left\{ \int_A p \cdot v_n^* dA \right\} \tag{3.14}$$

3.3 Equivalent radiated power

As explained in the last section, the radiated sound power can be calculated by the pressure and the velocity of an arbitrary fluid particle from the wetted surface. This implies that a fluid-structure coupling is required to obtain these values. However, such strong-coupling for large model which contains millions of DOFs usually takes too much time. To solve this problem, an alternative method called Equivalent radiated power (ERP) is employed. ERP is a simplified method to gaining information about maximal possible dynamic radiation of components and panels for specific excitations in frequency response analysis.

Assuming that each element from the wetted surface acts as a rigid piston, then the pressure in the equation can be replaced by the velocity according to equation 2.27 [1]

$$p = (\rho_0 c) v \tag{3.15}$$

Substituting into equation 3.14 then it is received

$$\mathsf{P}_{ERP} = \frac{1}{2} \rho c \int |v_s(x)|^2 d\Gamma(x) \tag{3.16}$$

Since the pressure term exists no longer, the computation can be performed with the uncoupled model. As a result, the requirements on computing power and computing time of optimization processes can be significantly reduced by using this method.

Chapter 4

Verification

In this chapter, some typical problems are considered in order to verify the presented methods such as reciprocity principle and equivalent radiated power. Different simple models are employed instead of the real model.

4.1 Reciprocity Principle in vibro-acoustics

For the purpose of the verification of reciprocity principle in vibro-acoustics, it is attempted to apply under three different situations and then observed, whether it performs well by these situations.

4.1.1 Simulation with fluid model

First reciprocity principle is tested with a absolute fluid model. The used model is quite simple and clear: A cuboid-shaped geometry is establish and meshed with 3D element CHEXA whose property is defined as a fluid. Two random points are chosen in the center part of the model, then an acoustic source is added at the first point and the generated sound pressure is measured at the second point (figure 4.1 left). After that, the function of these two points is changed, in other words, the position of the sound source and the receiver is switched (figure 4.1 right).

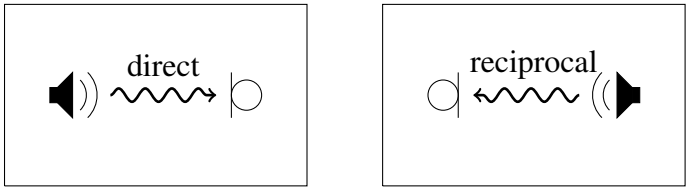

Figure 4.1: Reciprocal simulation with fluid model

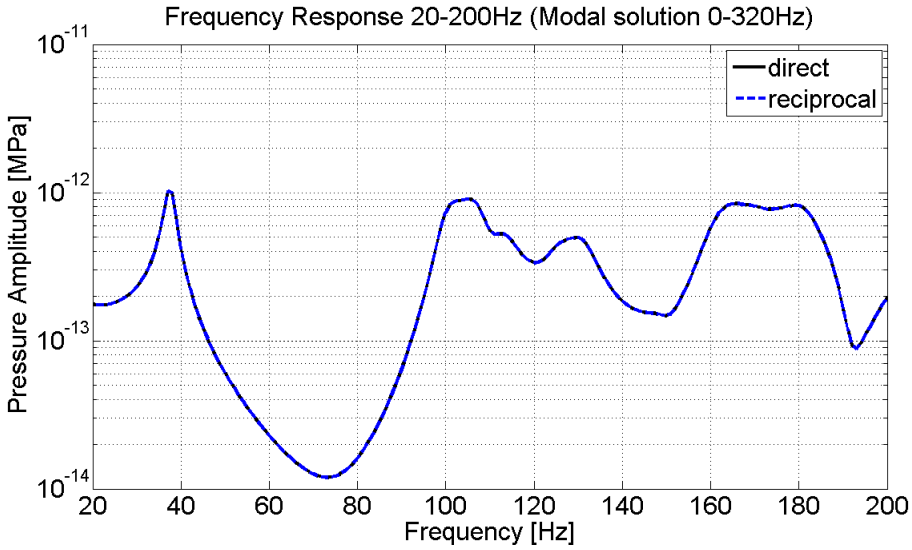

Figure 4.2: FRA for reciprocity principle with fluid model

The measured values are shown in Fig. 4.2 above, horizontal axis is frequency range and vertical axis represents the pressure amplitude in logarithmic scale. One can see clearly that curves of both calculation are coincident. This means if the source strength does not change, according to equation 2.52, the pressure will remain constant after the interchange of source and receiver.

4.1.2 Simulation with absorbing boundary with different impedance factor

In addition, the influence of the boundaries of fluid on the validity of reciprocity principle is also examined. Rayleigh implied in his work that the presence of locally reacting boundaries, or in other words, impedance boundaries, does not invalidate reciprocity. As mentioned in chapter 2.2.3, an impedance boundary conditions can be applied for the simulation. The same fluid model as last section is used, and a layer of absorbing elements is pasted on the surface of the fluid model refer to the process which is introduced in chapter 5.1 in detail. With the help of

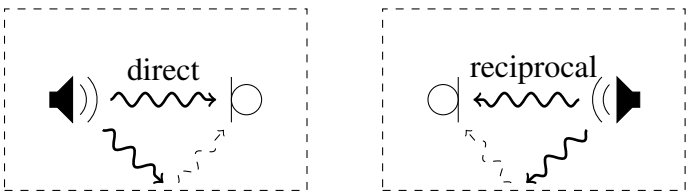

Figure 4.3: Reciprocal simulation with different impedance factor

Nastran one can create not only a completely absorbing boundary, but also a boundary which only absorbs part of the incoming wave and reflects the rest part. To observe the result under

different conditions, two calculation are computed and the impedance factors are set to 20% and 100% respectively. The results are displayed as following:

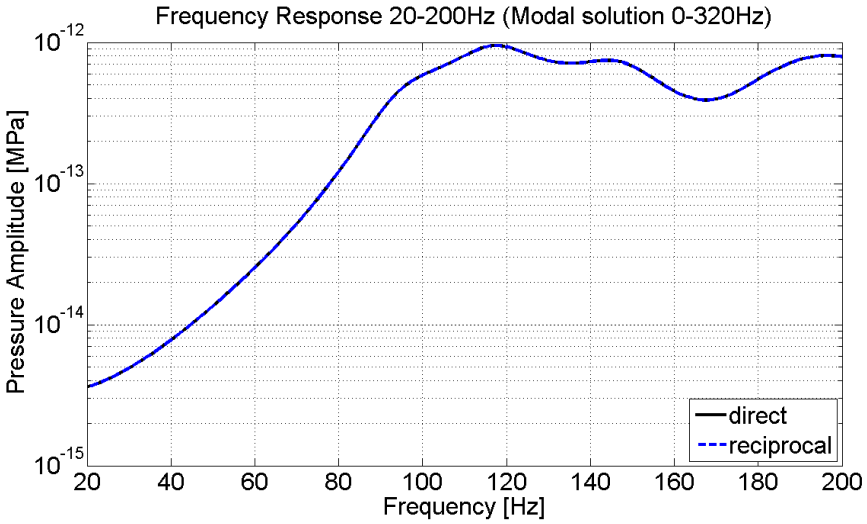

Figure 4.4: FRA for reciprocity principle with impedance factor 20%

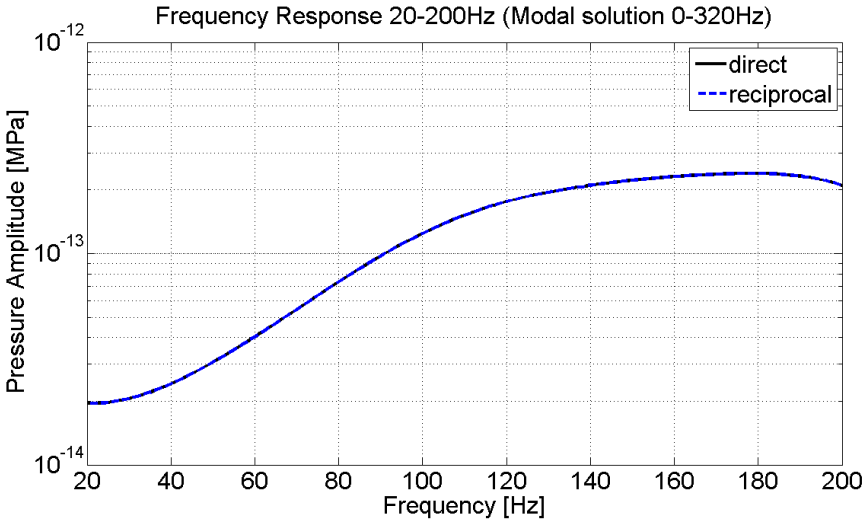

Figure 4.5: FRA for reciprocity principle with impedance factor 100%

Figure 4.4 shows the frequency response with a absorbing boundary condition with 20% impedance factor. There are less resonance frequencies compared with the original response without absorbing conditions, and the response curve becomes smoother, because the change of the boundary conditions reduce the number of the eigenfrequencies of the model. If the impedance factor is raised to 100%, it will lead to the result in Fig. 4.5. All the valleys and peaks exist no longer, but the reciprocity principle still holds true.

4.1.3 Simulation with FSI model & 2 measuring point/source

In the next step the reciprocity principle is tested on a fluid-structure interaction model. Moreover, the transfer function for multi-point is also tested together. The same fluid model is once again used, additionally the shell elements are created on two faces of the model as structure (see figure 4.6) and fluid-structure interface is automatically defined by Nastran. For strucutre the force F and velocity v take the place of the pressure P and source strength Q.

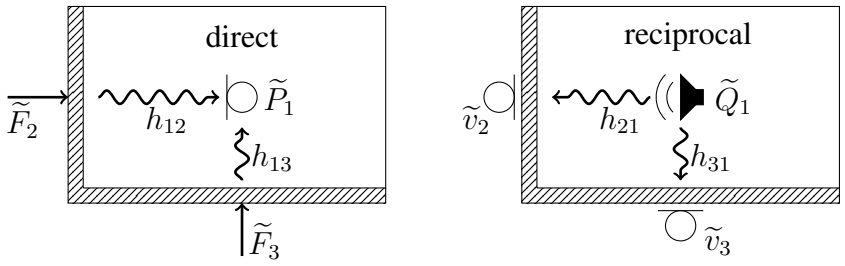

Figure 4.6: Reciprocal simulation with FSI model

This time only one point from the fluid model is chosen and it is numbered as point 1. Then two random points (point 2 & 3) are picked from each plate and given force excitation with amplitude $1N$ and $10N$ respectively. Of course the pressure at point 1 $\widetilde{P}_{direct}$ can be calculated directly. But alternatively one can also predict the response according to the Lyamshev reciprocity, one shall first recall

$$\frac{\widetilde{P}}{\widetilde{F}} = \frac{\widetilde{v}}{\widetilde{Q}}$$

consider that the total response is contributed by two sources, one receives the relationship

$$\widetilde{P}_1 = h_{12}\widetilde{F}_2 + h_{13}\widetilde{F}_3 \tag{4.1}$$

where h means the transfer function from source to receiver. From section 2.3.5 it is known that $h_{21} = h_{12}$, then

$$\widetilde{P}_1 = h_{21}\widetilde{F}_2 + h_{31}\widetilde{F}_3 = \frac{\widetilde{v}_2}{\widetilde{Q}_1}\widetilde{F}_2 + \frac{\widetilde{v}_3}{\widetilde{Q}_1}\widetilde{F}_3 \tag{4.2}$$

therefore the so-called "reciprocal solution" is needed (figure 4.1 right). Setting a sound source with unit source strength $Q_1 = 1[mm^3/s]$, then the generated velocity from point 2 and point 3 is measured and substituted into equation 4.1. Finally the calculated result is compared with the direct solution.Figure 4.7 shows that the response curve looks like the same one with each other. This proves that the reciprocity principle is also valid for fluid-structure interaction situations.

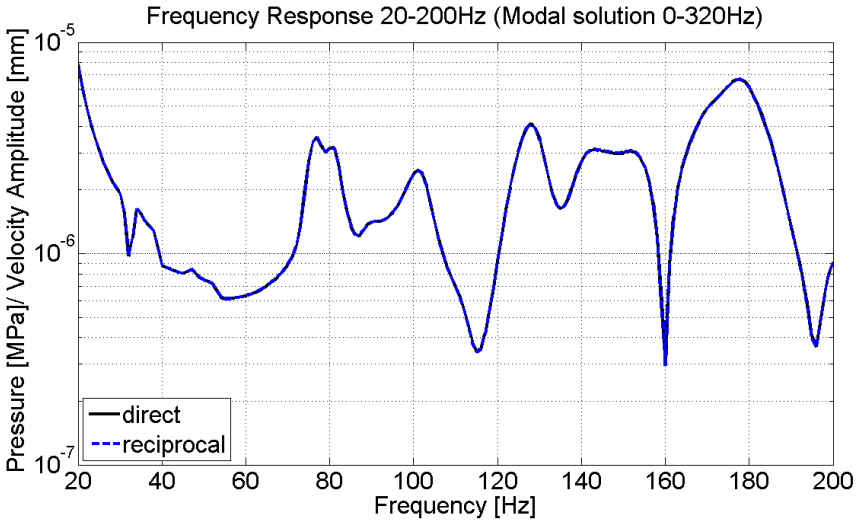

Figure 4.7: FRA for reciprocity principle with FSI & 2 measuring point/source

4.2 Acoustic power & ERP

In this section the acoustic power radiated from the vibrating structure as well as the equivalent radiated power ERP are evaluated. Several solutions are chosen in order to verify the performance of both methods. And Nastran provides many kinds of solutions to handle such problems. All these available solutions supported by Nastran are listed in table 4.1 with different outputs.

Node Solutions	Panel Solutions
Intensity	Acoustic Power
Pressure	Equivalent Radiated Power
Velocity	

Table 4.1: Solutions supported by Nastran

Again a simple model is used to satisfy the requirement. A fluid model with cuboid geometry is employed. Shell elements are created on one side of the fluid model. A time-harmonic force is added as vibration source in the middle of the structure (see figure 4.8). Any other settings in detail see also Chapter 5.1 .

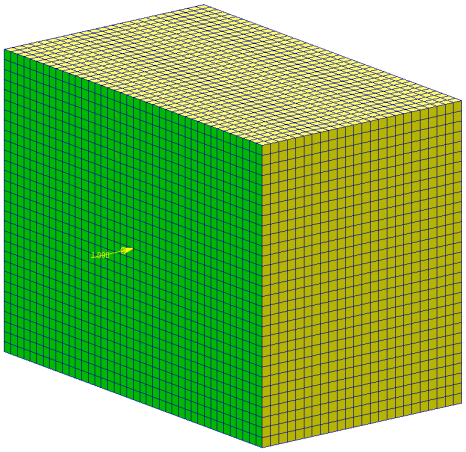

Figure 4.8: Simple model for ERP

4.2.1 Acoustic Power

For the purpose of discussing the validity of acoustic power, it is necessary to get a clear idea how these values are calculated. By Nastran one can request output of the power radiated from the wetted surface with command ACPOWER (refer to [6] P.434). Meanwhile, from equation 3.14 it is known that the integral of intensity over the surface provides the acoustic power. To calculate the intensity, one need first gather the pressure and velocity data from the wetted surface.

Since the structure mesh and fluid mesh are coincident by this model, through MATLAB one can easily read the coordinate information for each solid node and find the corresponding fluid node on the interface. Thus it is possible to obtain the intensity according to equation 3.13. After that, both the calculated intensity and the intensity direct from Nastran are plotted as following:

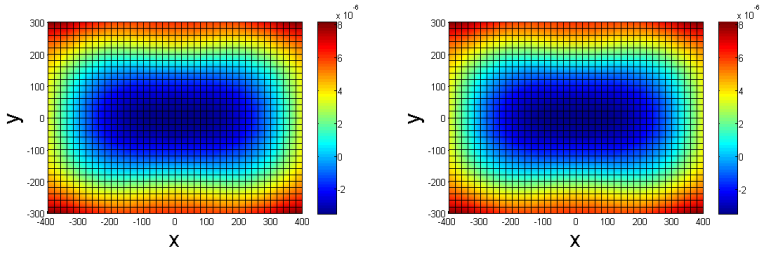

(a) intensity results from calculation (b) intensity results direct from Nastran

Figure 4.9: Comparison of intensity results for 20 Hz

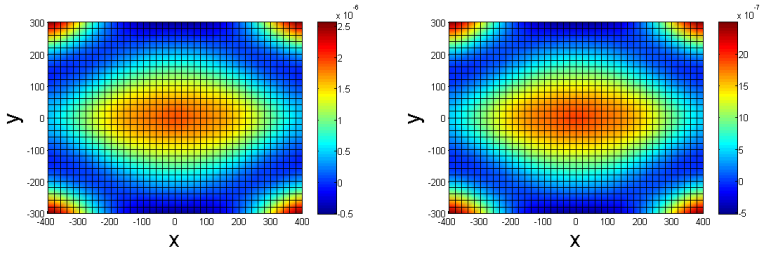

(a) intensity results from calculation (b) intensity results direct from Nastran

Figure 4.10: Comparison of intensity results for 200 Hz

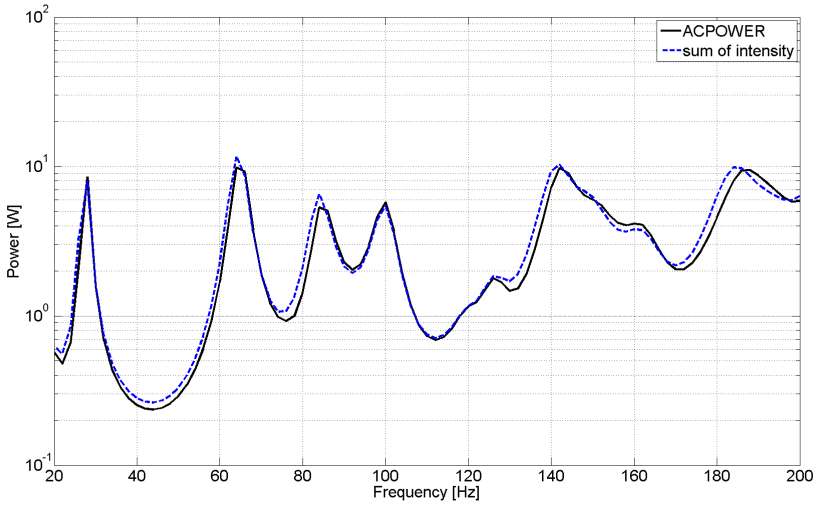

Figure 4.11: Comparison between ACPOWER and integral of the intensity

Figure 4.9 and 4.10 show that the calculated intensity is almost the same as the intensity direct from Nastran. Next step the intensity is integrated over the whole area of the surface and then compare with the result which is received direct by ACPOWER command (see figure 4.11). The relation between intensity and acoustic radiated power is proved to be true, although there is still some deviation between two curves which can be interpreted as the error caused by different interpolation method.

4.2.2 ERP

Then equivalent radiated power is also tested with the same model in a similar way: The velocity response of the structure is first measured and an analog intensity is calculated for each solid node from the wetted surface according to equation 3.16. After this ”equivalent” intensity

is integrated over the area, it will be compared with the ERP results direct from Nastran output. Figure 4.12 shows both results agree with each other perfectly.

Finally, the ACPOWER results and ERP results are illustrated in Fig. 4.13. One can see that two results differ greatly in value. However, it can be found that the shape of two curve are similar in general, peaks and valleys in the curves are found almost at the same frequencies.

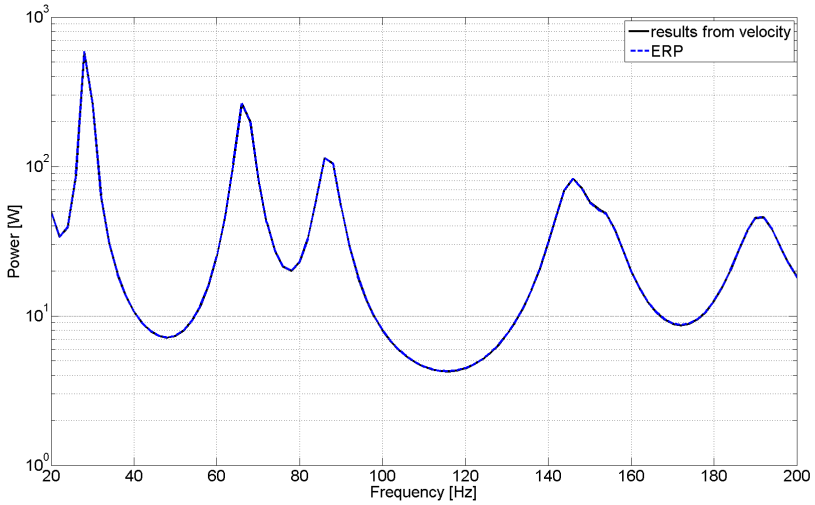

Figure 4.12: Comparison between ERP and result calculated from velocity

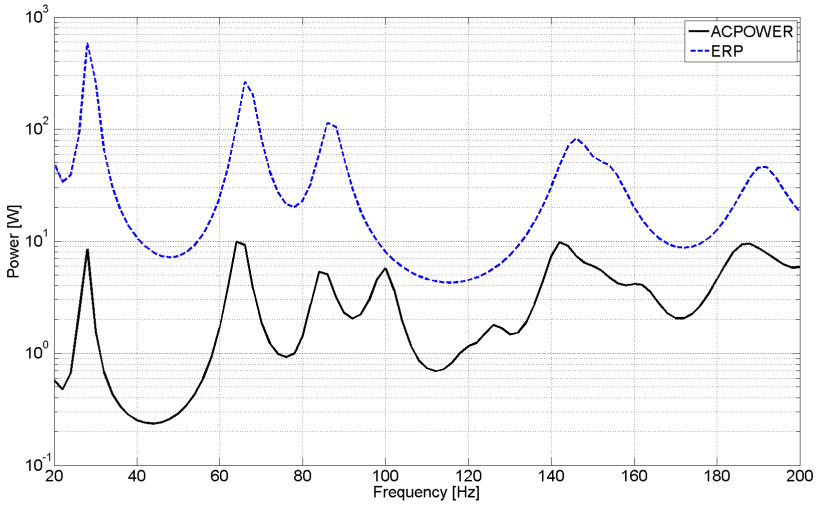

Figure 4.13: Comparison between ERP and ACPOWER

On the other hand, the time cost for the simulation is also considered. The time cost of ACPOWER and ERP solution is listed in the following table 4.2. The frequency range is between 20 Hz and 200 Hz, containing 91 frequency steps. For both direct solution and modal solution the computing cost is greatly reduced by using ERP method

	ERP modal	ACPOWER modal	ERP direct	ACPOWER direct
Degrees of Freedom	7626	39401	7626	39401
Structure Modes	41	41	-	-
Fluid Modes	-	196	-	-
Real Time	4.0s	43.6s	12.1s	1532.2s
User Time	1.1s	38.5s	9.2s	1511.8s
System Time	0.3s	2.6s	0.9s	18.0s
Disk Usage	49.1Mb	509.9Mb	42.4Mb	459.7Mb
Memory Usage	3497.2k	26843.2k	2707.1k	21095.2k

Table 4.2: comparison of the time cost for different solutions

Chapter 5

Applications

In this chapter a practical application provided by company Airbus is presented. The model will be first introduced and the SPL response is predicted over a given frequency range with the help of Nastran. After that, based on the results from evaluation methods the structure is modified according to the optimization process.

5.1 Modeling

In this study, a 1/2-scale model of the rear part of an airplane, which consists of the tail and a section of the fuselage, is used. The assembly model is shown in figure 5.1. The following subsections highlight the mesh details of the airplane model.

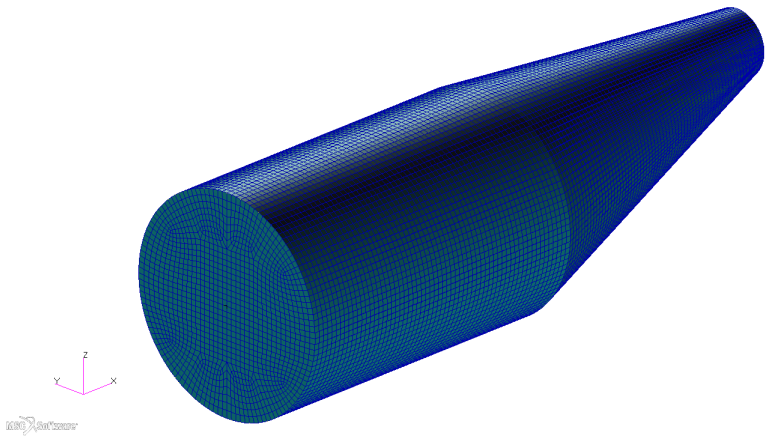

Figure 5.1: The FE-model

5.1.1 Material

The aviation industry mostly employs aluminium alloys for airplane hulls because of their outstanding physical properties, good machinability and malleability. For this reason, most structure parts in this model are assumed to be made of aluminium. Furthermore, a honeycomb and resin material is used in other regions.

For fluid elements one shall use the material properties of air. Considering that the dimension of the model is scaled by the factor 1/2 and due to

$$f = \frac{\lambda}{c}$$

the speed of sound needs to be halved in order to keep the frequency f constant. The resulting material properties are listed in table 5.1.

Structure	Young's modulus	Poisson's ratio	Density
Aluminium	7.3e10 N/m^2	0.34	2700 kg/m^3
Structure	Young's modulus	Poisson's ratio	Density
Honeycomb	3.0e7 N/m^2	0.2	48 kg/m^3
Resin	Longitudinal modulus	Lateral modulus	Shear modulus
HTA/977-2	1.352e11 N/m^2	9.3e9 N/m^2	4.88e9 N/m^2
	Poisson's ratio	Density	
	0.34	1600 kg/m^3	
Fluid	Bulk modulus	Speed of sound	Density
Air	35836 N/m^2	170 m/s	1.24 kg/m^3

Table 5.1: Material parameters

5.1.2 Structure model

The structure can be geometrically decomposed into a cylinder and a truncated cone. These two parts are named S18 and S19, respectively. Figures 5.2 and 5.3 show cross sections along x-axis of each part that reveal their internal structure.

Structure of S19

S19 primarily consists of an external skin in the shape of a truncated cone. This skin is defined as quadrilateral plate element CQUAD4 with a thickness of 4 mm. Thus to check the quality of

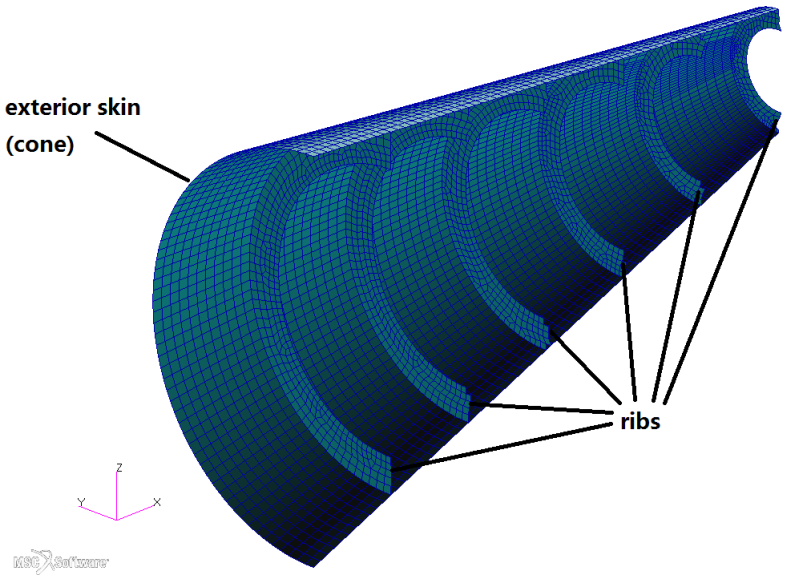

Figure 5.2: Cross-section view of S19

FE models, one can calculate the wavelength of bending waves in plates and compare it with the element size. For a plate of thickness $h = 4mm$, using the material properties of aluminium from table 5.1, the bending rigidity evaluates to

$$D = \frac{Eh^3}{12(1-\nu^2)} = \frac{7.3 \cdot 10^{10} \cdot (0.004)^3}{12 \cdot (1-0.34^2)} Nm = 440.2Nm$$

the highest frequency leads to the shortest wavelength. For the maximal frequency $f_{max} = 200Hz$ the wavelength is

$$\lambda_B = 2\pi \sqrt[4]{\frac{D}{\rho h}} \frac{1}{\sqrt{\omega}} = 2\pi \sqrt[4]{\frac{440.2}{2700 \cdot 0.004}} \frac{1}{\sqrt{2 \cdot pi \cdot 200}} m = 0.4478m = 447.8mm$$

at least 8 elements are required per wavelength, which means the maximal length for each edge should be about 55 mm. And most elements in this model satisfy this requirement.

In addition, there are 6 reinforced ribs in the interior side of the skin, whose task is to improve the stiffness of the structure. These ribs are also made as CQUAD4 elements but with a thickness of $h = 3mm$.

Structure of S18

A special element type is used in some component of S18. The parts ”partition wall” and ”floor” are constructed by a stuff which is called composite laminate, which are commonly used in

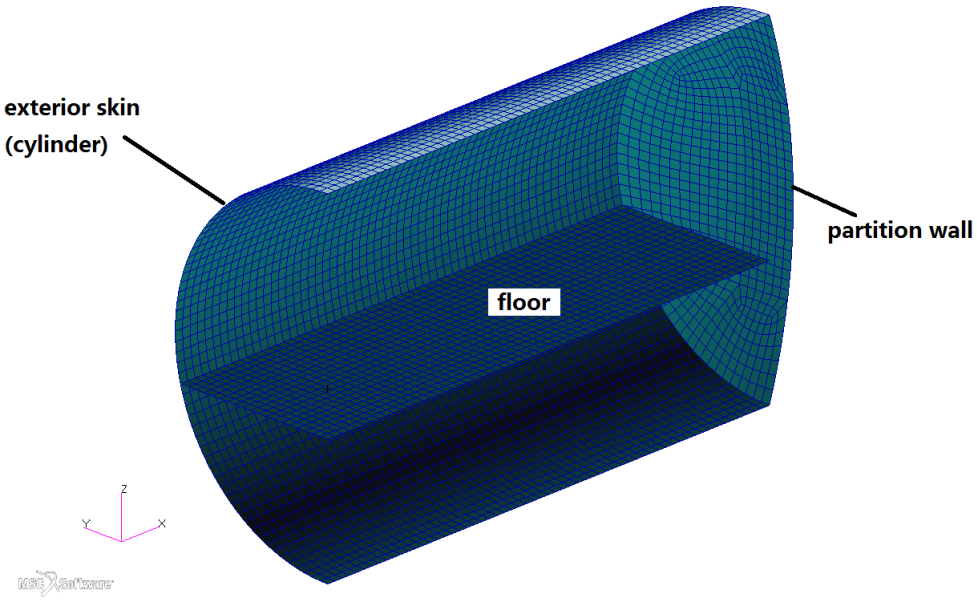

Figure 5.3: Cross-section view of S18

modern aircraft manufacturing. Composite laminates are manufactured by combining layers of material together. Each layer of material is called a ply, and each ply is arranged to have a certain angle so that the entire laminate resistance obtain the resistance against deformation from all the directions. A typical example of composite laminate is shown in Fig. 5.4.

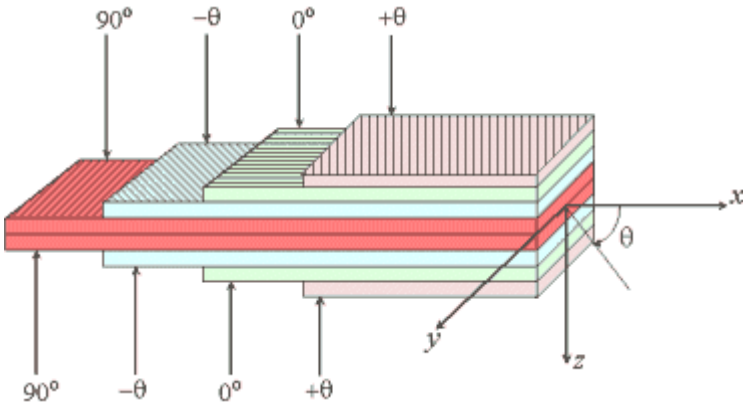

Figure 5.4: An example of a composite laminate [17]

In Nastran one can use layered composite element PCOMP to define the properties of an n-ply composite material laminate.

Region ”partition wall” is consist of 20 plies with Resin HTA/977-2. Each ply has equal thickness and different directions. The total laminate thickness of the partition wall is 2.94mm.

The ”floor” consists of 18 plies, where the two innermost plies are made of honeycomb material with a thickness of 8 mm while the other plies are made of resin HTA/977-2 with a thickness of 0.147 mm. The total laminate thickness of the floor is 18.352 mm.

The exterior layer of S18 is similar to S19, only thinner with $d = 3mm$. In addition, some beam elements are established on the side surface of the cylinder. Stringers are built along the x-axis while frames are built along the circular direction (see figure 5.5). They function as stiffener and also part of the exterior. In Nastran they are modeled by CBAR elements with a box-shaped cross section.

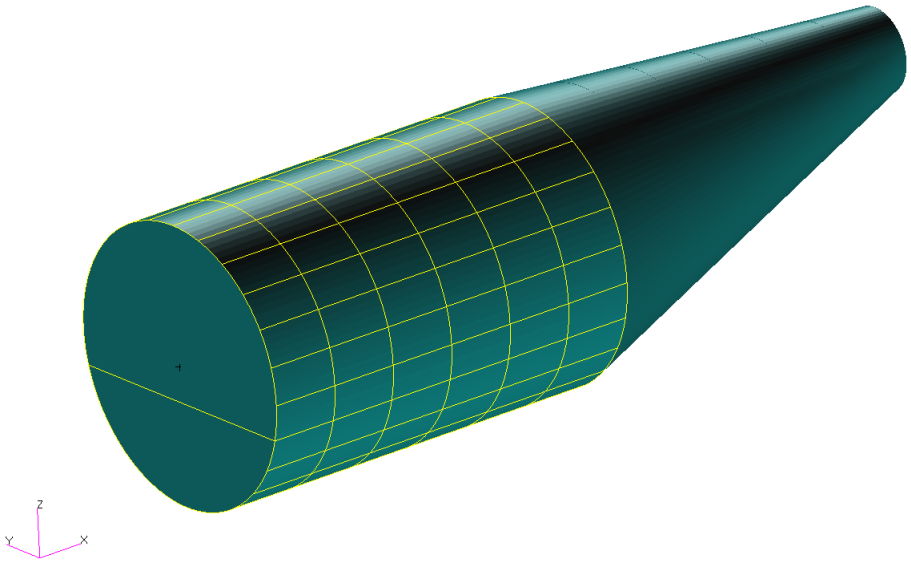

Figure 5.5: stringer and frames

5.1.3 Fluid model & boundary conditions

There are three fluid bodies in this model: The fluid body inside the hull structure S19 and the two fluid bodies in S18 (above and under the floor). In this study we mainly focus on the passenger cabin, which is located between the floor and the upper hull. The cabin is modeled in Nastran by a six-sided solid element CHEXA (see figure 5.6).

Again the wavelength is checked for the sound wave

$$\lambda = \frac{c}{f} = \frac{340}{200}m = 1.7m$$

The wavelength is far larger than the plate dimensions. The quality of the mesh is therefore acceptable.

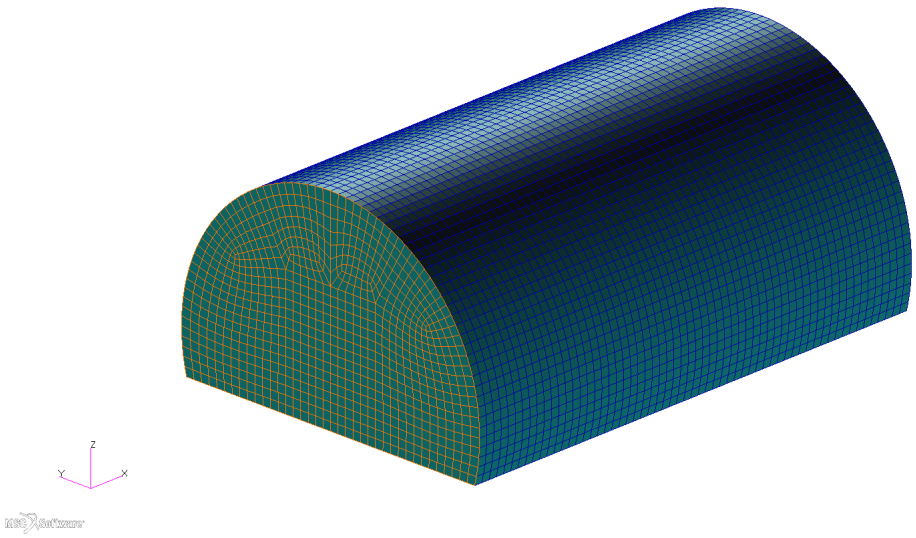

Figure 5.6: Fluid cabin model

Considering this fluid model is only one section of the whole cabin. This means when the sound wave reach the border of the fluid model, it should not be reflected by the boundary but propagate forward. By using the absorbing boundary conditions refer to section 2.2.3, a layer of CAABSF elements are created on the selected surface (the orange selection in Fig. 5.6) to eliminate the unwanted reflections. In this way the sound propagation of a full-sized cabin is simulated.

As a summary, the number os elements and their types are listed in table 5.2. The number of elements determines the number of nodes and thus the DOF. Therefore the CHEXA elements, namely fluid elements contribute about 55% DOF of the whole model. And the remaining DOF mostly belong to the shell element CQUAD.

CAABSF	1352
CBAR	2546
CHEXA	170352
CQUAD	21747
GRID	204954
DOF	313509

Table 5.2: The number for different elements

5.1.4 Loads & measuring points

In order to perform the frequency response analysis a dynamic load is needed. To simulate the actual loading conditions, a harmonic force vibration is placed at node 8373, on the exterior of S19 (the yellow arrow in Fig. 5.7) as excitation.

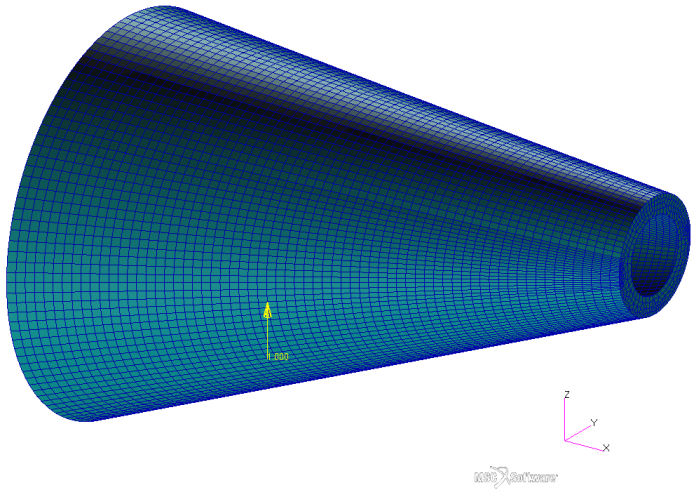

Figure 5.7: sound source on the structure

On the other side, the measuring points are at the locations where passengers are likely to perceive it. These locations depend on the arrangement of seats, which is provided by Airbus. There are 7 rows and 6 lanes, 42 seats altogether. The space between each row is 60 cm and 80 cm for each column. The sketch of the ear positions of passengers are illustrated in Fig. 5.8.

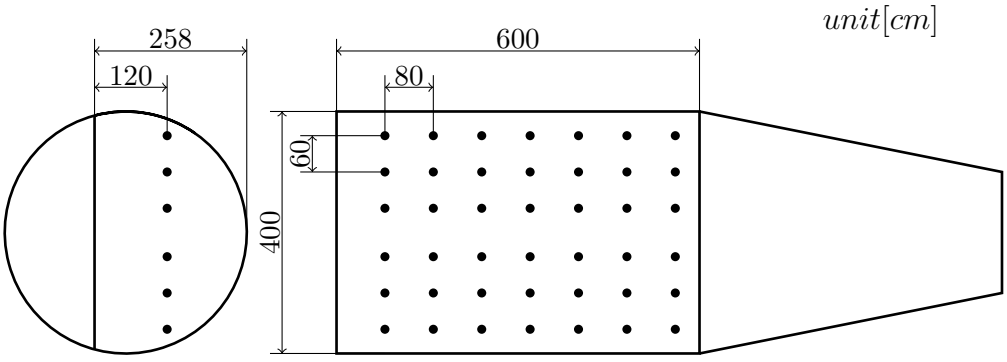

Figure 5.8: Sketch of ear positions in the cabin

There is a problem for picking these points: Because the fluid model is not specially meshed for the ear position, it is impossible to locate the desired place precisely. To solve this problem,

a short MATLAB program is applied to search for the nearest node from the FE model. These nodes are shown in the following figure:

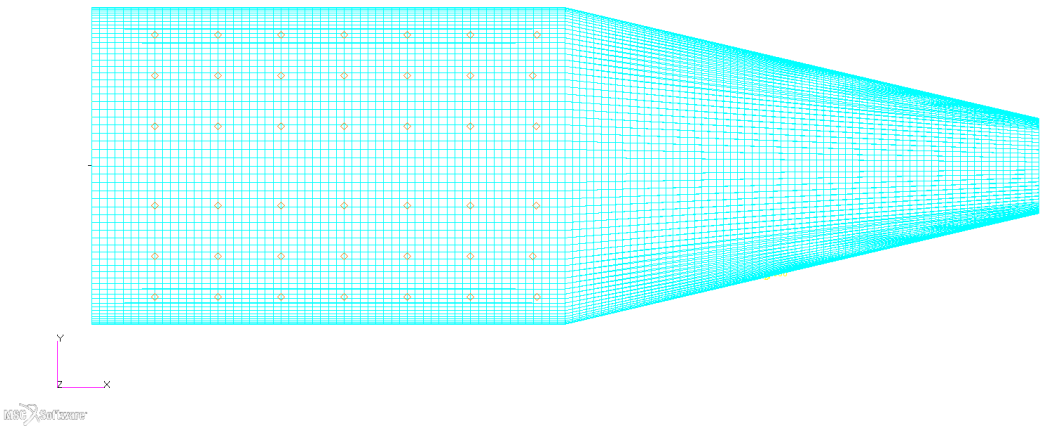

Figure 5.9: Chosen nodes for ear position

Moreover, the modeling parameters for fluid-structure interface is defined by ACMODL command. The interface type DIFF with searching algorithm BW is selected so that the fluid nodes and solid nodes on the interface will be found and coupled automatically. Finally, with all these information the calculation can be performed by Nastran. The complete Nastran command file is printed in appendix.A

5.2 Results of the original model

After the calculation is done, Nastran will output the results to a .pch file, from which it can be read directly by Matlab. The results from the original model are presented in the following sections and provide a starting point for further optimization.

5.2.1 Sound pressure level (SPL) analysis

At first the sound pressure levels for all measuring points in the range of acoustic frequencies of interest are shown in Fig. 5.10. The plots correspond to the 42 ear positions with the same arrangement.

It is feasible to analyze the response for each ear position. For simplicity, the global result which is obtained by averaging all the local results is mainly concerned. This averaged SPL is shown in the following figure

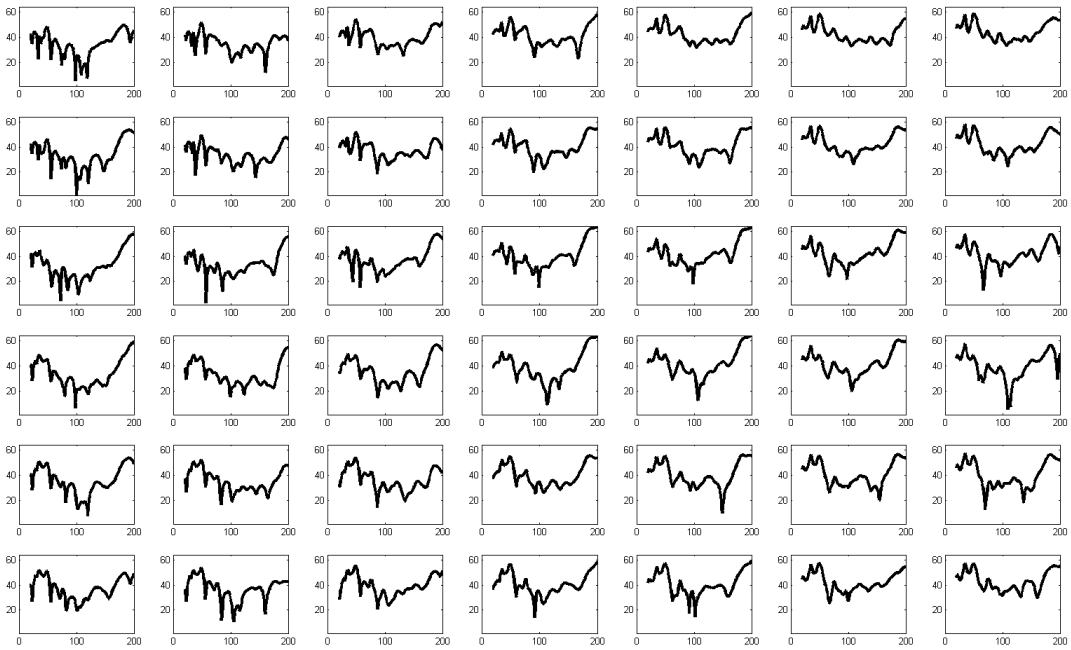

Figure 5.10: SPL result of original model for each subcase

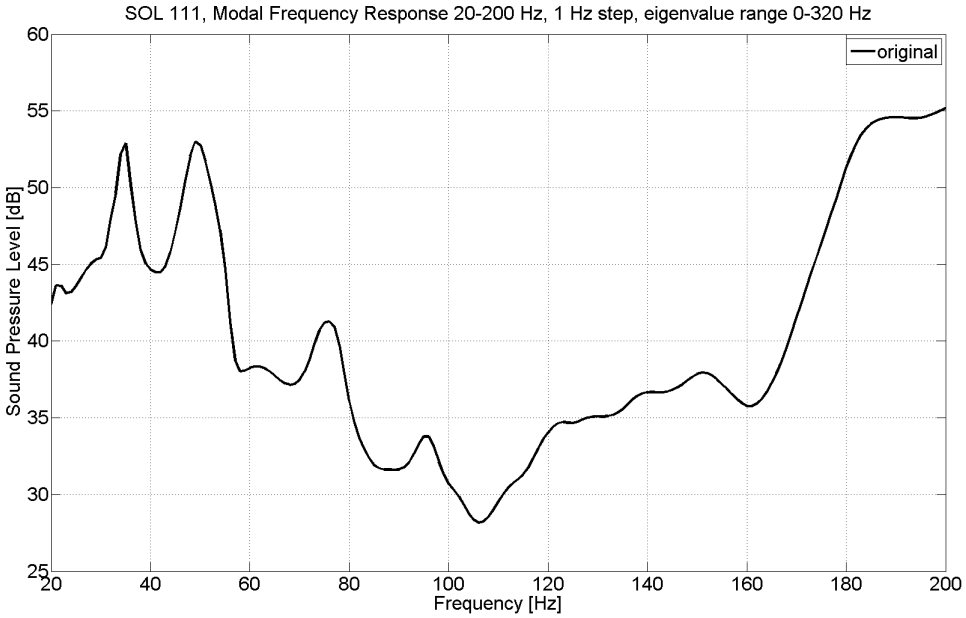

Figure 5.11: Averaged SPL result of original model

In this graph, the loudness peak can be observed from the response curve. Two obvious peaks exist at frequencies 35 Hz and 49 Hz. A weaker peak is located at frequency 76 Hz. There is an overall increase in SPL in the higher frequency range, where 190 Hz is selected for observation.

5.2.2 Panel participation

For the purpose of identifying the structure region that has the biggest contribution on the response, the panel participation factor is applied. In order to perform this calculation, first it is necessary to define the panels from the wetted surface. It is divided into 4 regions: cylinder left, cylinder right, partition wall and floor (see figure 5.12).

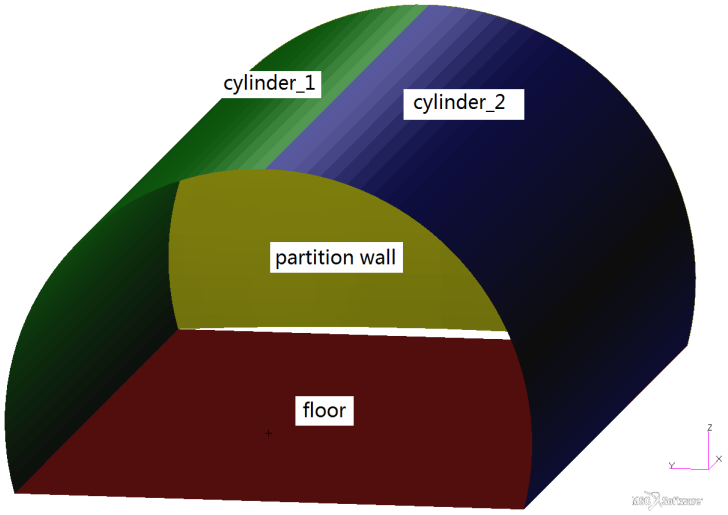

Figure 5.12: Definition of panels

The panel participation factor estimates the most influential region at a certain fluid node. In this investigation, the panel participation factor is computed for each ear position. After that, the results are averaged for all 42 subcases and then discussed. figure 5.13 shows the averaged absolute value of panel participation factors over all frequencies. From the graph one can observe that the curves for the left cylinder and the right cylinder are similar to each other. Over most of the frequency range, the floor region is the most influential. For the lower frequencies, the contribution from the partition wall is below other panels.

One shall not just pay attention to the amplitude of the panel participation factors. As a matter of fact, The panel participation factor is a complex number and the total pressure response is formed by the complex-valued superposition of the contribution from all panels. That means, the result is not only determined by the absolute value, but also the phase differences of the panel participation factors of all panels. Therefore, in the following figures (5.14 to 5.17) the complex-valued panel participation factors are depicted as arrows in the complex plane for each peak frequency.

It is observed that the panel ”floor” always plays an important role for most peak frequencies

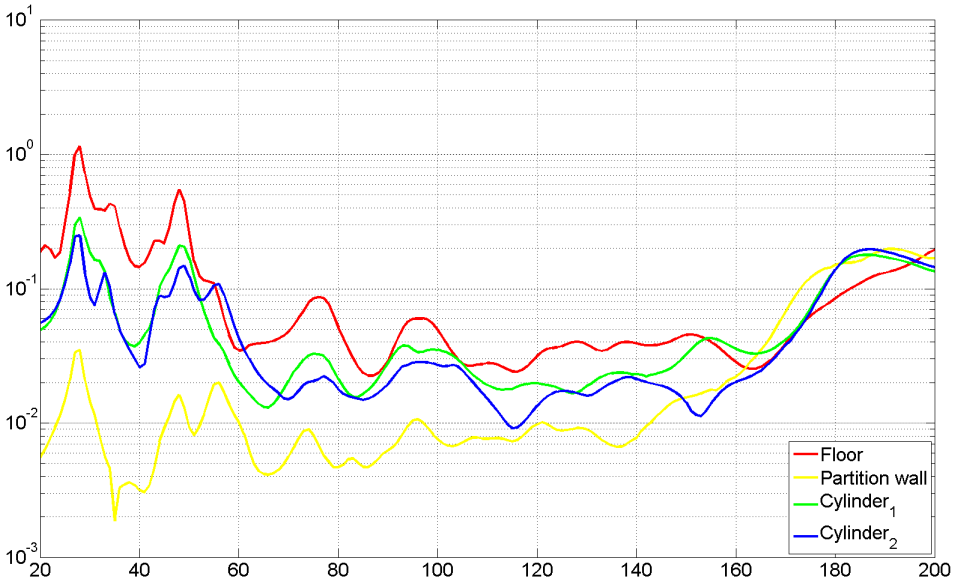

Figure 5.13: Panel participation factors in the range 20-200 Hz

except for frequency 190 Hz. This circumstance may be used for further optimization.

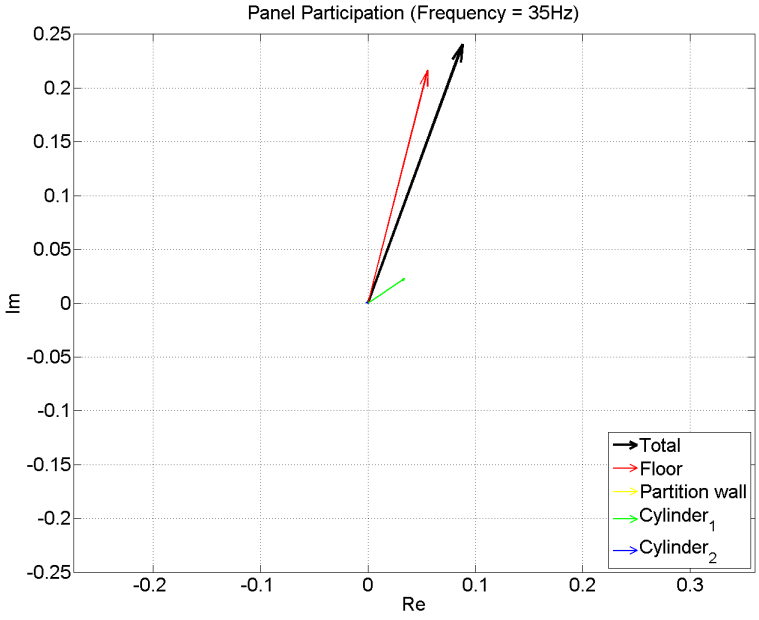

Figure 5.14: Panel participation factor for 35 Hz

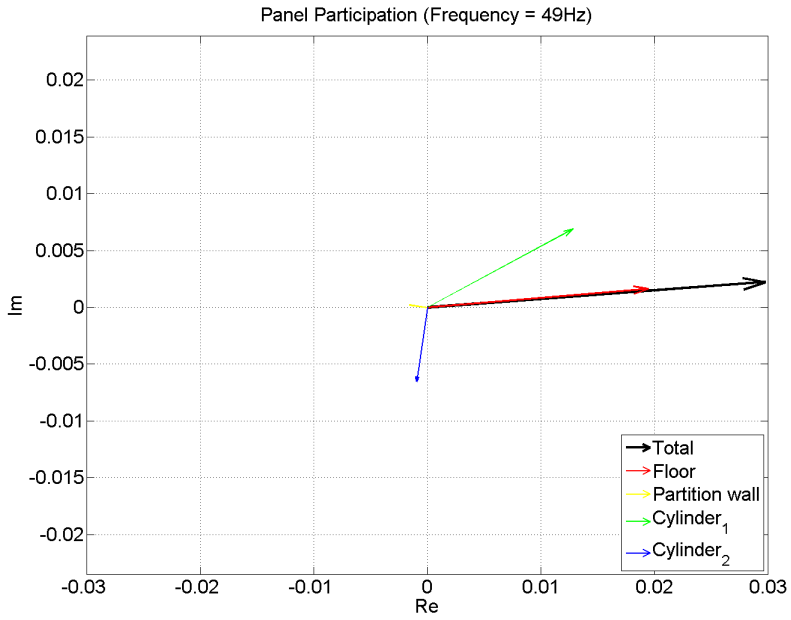

Figure 5.15: Panel participation factor for 49 Hz

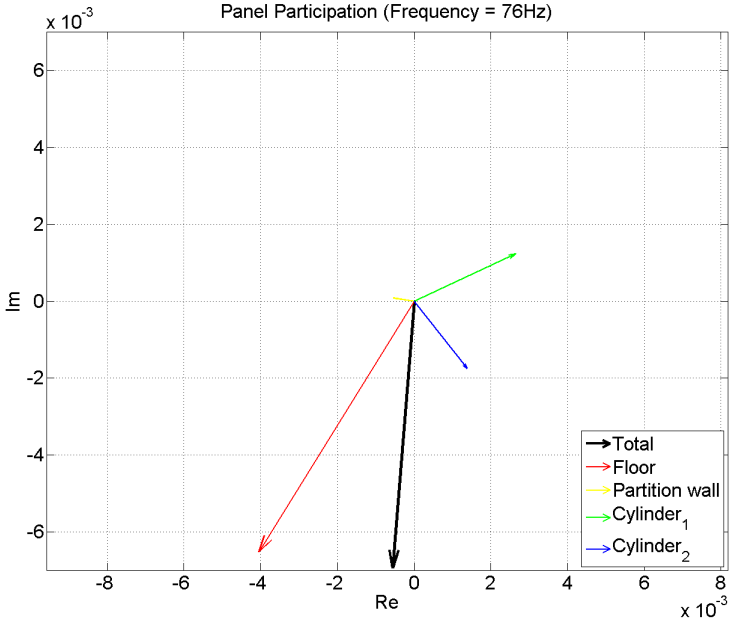

Figure 5.16: Panel participation factor for 76 Hz

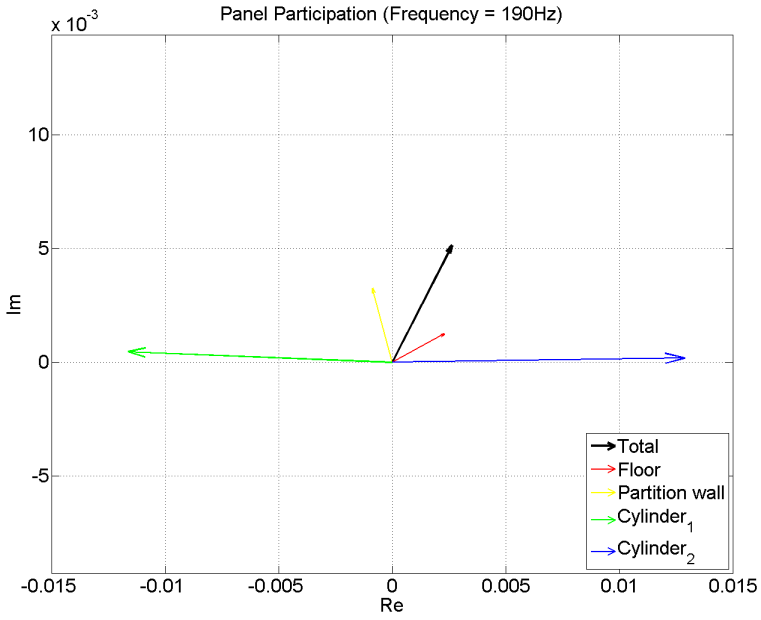

Figure 5.17: Panel participation factor for 190 Hz

5.3 Optimization

To improve the dynamic characteristic of a system, the common method is either to increase the stiffness through additional mass or reduce the mass of the structure. However, for the aviation industry every added weight on the structure means the loss of economical efficiency. As a result, engineers are required to improve their designs by using stiffer and, at the same time, lighter parts. To meet these requirements it is necessary to use efficient methods for discovering the weak points of a structure.

At this point, the alternative method—reciprocity principle is employed. Through the study of reciprocity principle one can know that the sound pressures generated at the ear positions of passengers can be estimated by measuring the vibration at the actual source position caused by an acoustic sources at the ear position according to the Lyamshev reciprocity (see also the example in section 4.1.3). Further more, one may conjecture that those regions whose response is larger than others in the reciprocal calculation will transfer more vibrational energy in the direct calculation. Through modifications in these sensitive regions we can reach the objective of reducing the noise at the receiver.

5.3.1 Tuned mass damper

After analyzing the weak point of the structure, measures should be taken for the optimization. In this study, structure is optimized by making use of tuned mass dampers. The tuned mass damper, also known as harmonic absorber, is a device mounted in structures to reduce the amplitude of mechanical vibrations [15]. A schema of a typical tuned mass damper is shown in Fig. 5.18.

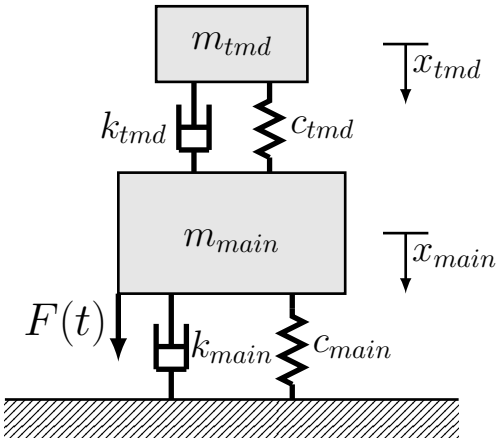

Figure 5.18: Tuned mass damper

The main mass m_{main} is mounted by spring k_{main} and damper c_{main}. The force on the main system is $F(t)$. The tuned mass damper with mass m_{TMD} is attached to the main system with spring k_{TMD} and damper c_{TMD}. The mass of the damper depends on the mass of the system being damped and is customarily 10% of the main mass. The eigenvalue of the damper system is specified by the equation $f = \sqrt{k/m}$ (generally the mass is constant and the stiffness is adjusted), so that the damper system vibrates at the same frequency as the main system but with a phase shift and thus reduces the response of the system at the peak frequency.

figure 5.19 shows the effect of a tuned mass damper on a simple system, which is excited by vibrations applied to the main mass. One can observe that the damping has a significant effect on the frequency response. Changing the damping decreases the sensitivity at resonant frequencies and also changes the height of the peaks. For this reason it is important to choose a suitable damping coefficient for the optimization.

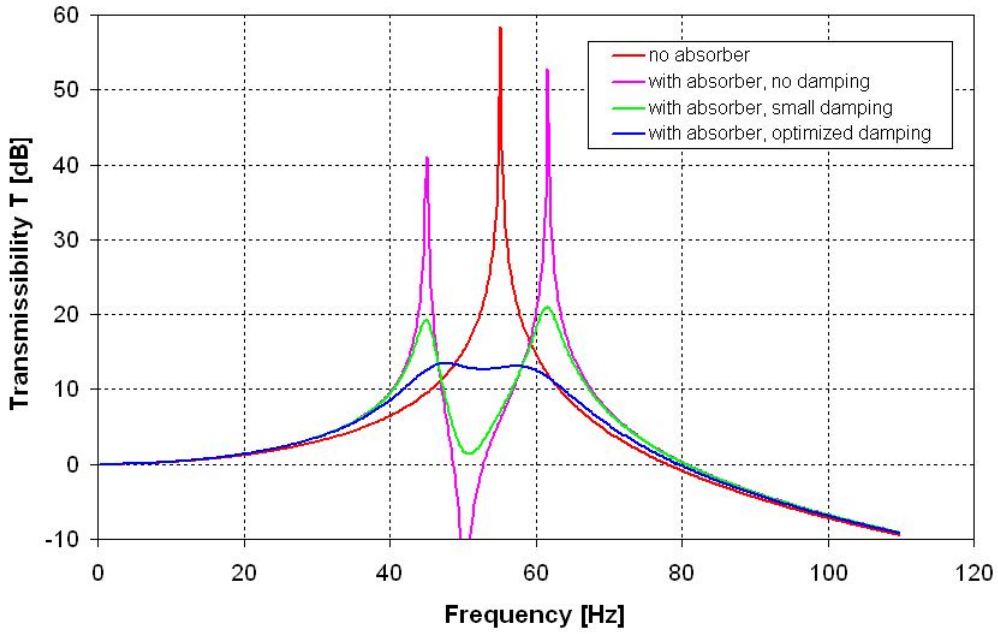

Figure 5.19: An example of tuned mass damper [15]

5.3.2 Optimization on S19

To perform the optimization on the structure, the reciprocity principle is applied at first . And the sound source in this model is no more an excitation on the structure, on the contrary, it is de-

fined as a point source placed at the ear position. And the transfer function between the source and the receiver is calculated for each ear position. For this reason 42 subcases are needed to obtain the transfer functions for all ear positions.

In Nastran, an acoustic point source in the fluid model is specified by the command ACSRCE. The source strength Q is defined as a function of the frequency f [7]

$$Q = A \cdot \left[\frac{1}{2\pi f} \sqrt{\frac{8\pi C P}{\rho}} \right] e^{i(\theta + 2\pi f \tau)}$$

which means the source strength Q will change with the frequency. Specially, the Power P can be specified as a quadratic function of frequency

$$P(f) = \frac{\pi}{2} \cdot \frac{\rho}{C} \cdot f^2$$

so that the dependency of the magnitude on f can be eliminated. Thus, an acoustic source with constant source strength for the whole frequency range is obtained.

After the numerical results are computed, A Matlab program (see appendix C) is used to visualize the sensitive areas in the structure. The responses for all solid nodes are read from .pch file and averaged. Attributes of the node elements, such as location and identification number, are read from the model file and matched with the computation results so that it can be plotted in Matlab.

In order to simulate the tuned mass damper in Nastran, the CONM2 element is used to define the additional concentrated mass at a grid point. This mass elements is connected with the main structure by using a spring-and-damper element CBUSH, whose property is specified by the command PBUSH.

In the last step, the response is computed once again and the obtained results are compared with the original results. In the following sections such comparisons are done for four peak frequencies. A Nastran example is listed in appendix.B.

Optimization for 35 Hz

From figure 5.21 one can see that the sensitive areas are primarily at the top of S19. Using tuned mass dampers in these locations results in the response behavior shown in Fig. 5.22. Compared to the original SPL response, the response after this modification shows decreased pressure levels at 35 Hz.

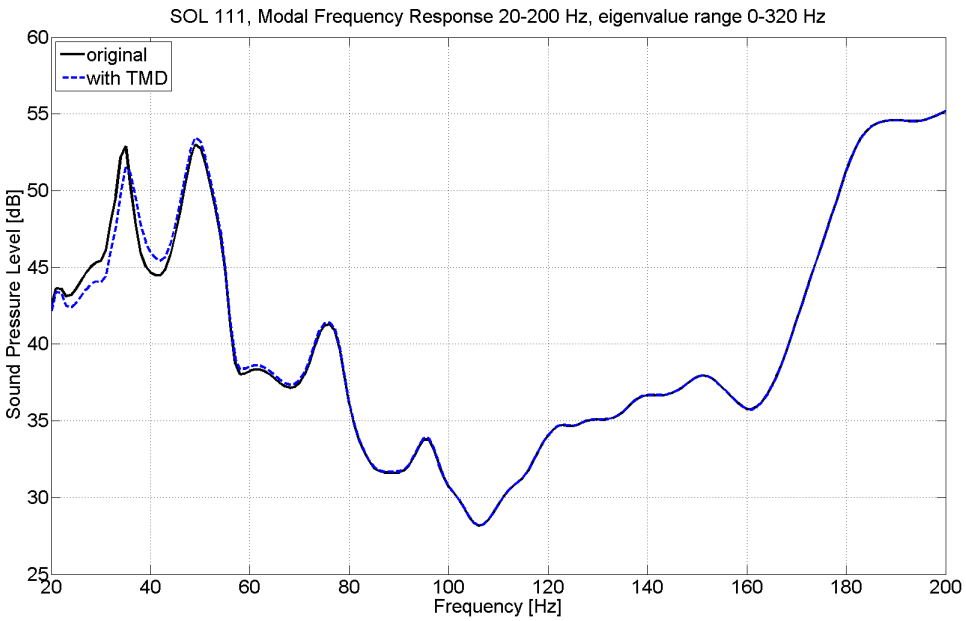

Figure 5.20: SPL comparison between the modified model (for 35 Hz on S19) and the original model

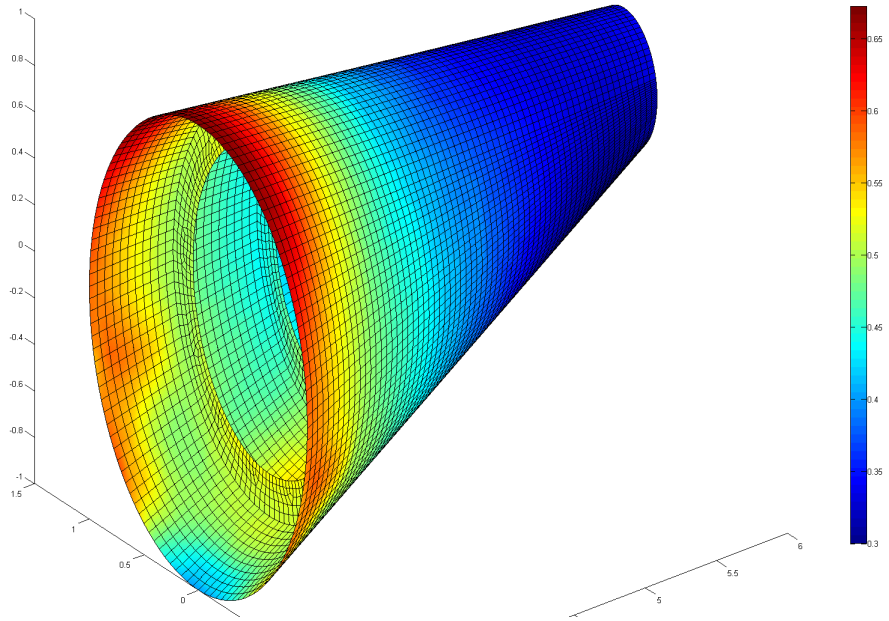

Figure 5.21: Response at 35 Hz before the modification on S19

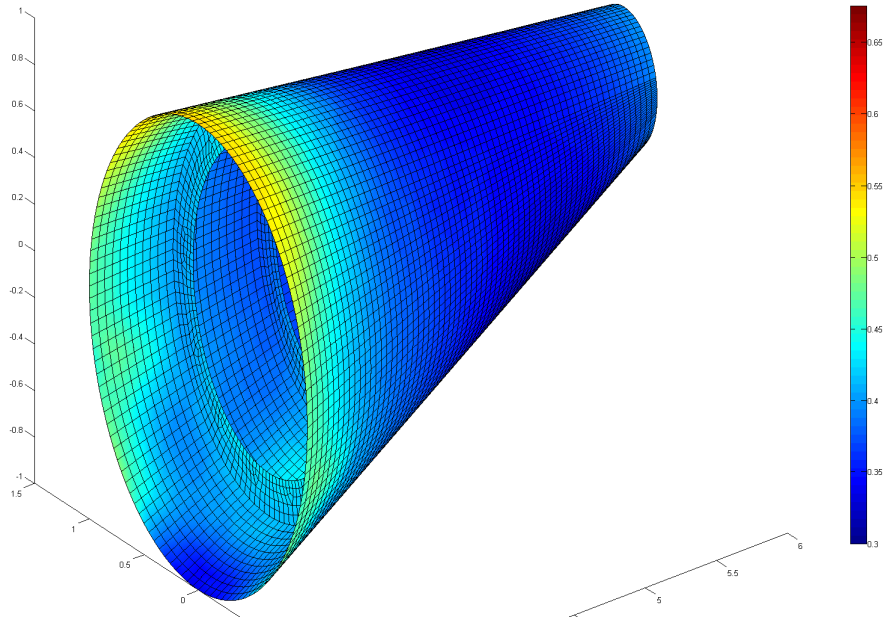

Figure 5.22: Response at 35 Hz after the modification on S19

Optimization for 49 Hz

For 49 Hz, the sensitive area is similar to the one for 35 Hz (see figure 5.24). The comparison with the original frequency response in Fig. 5.25 shows that the effect of the modification is not as visible. There is a slight decrease on the response curve at frequency 49 Hz.

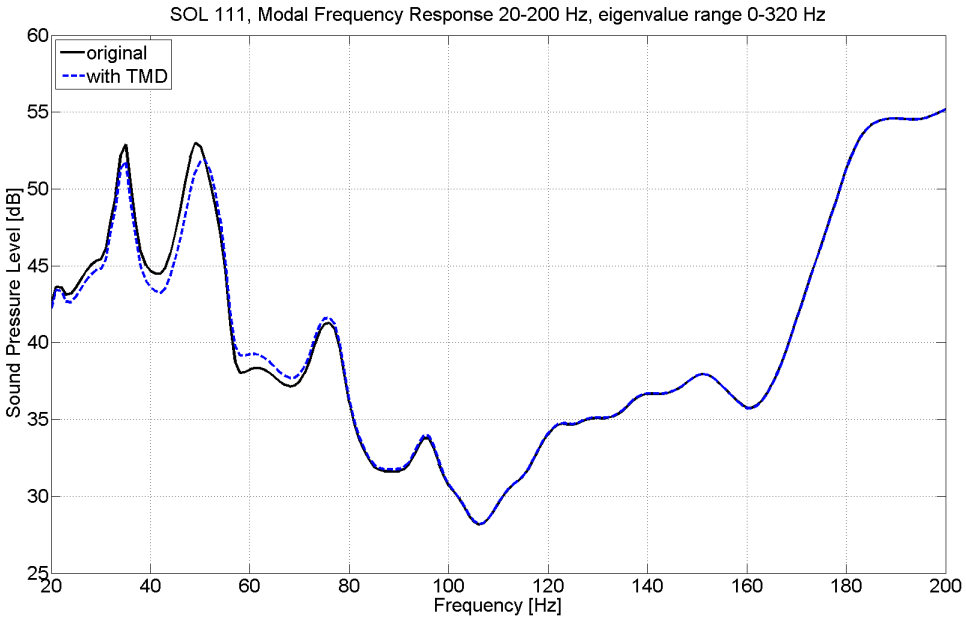

Figure 5.23: SPL comparison between the modified model (for 49 Hz on S19) and the original model

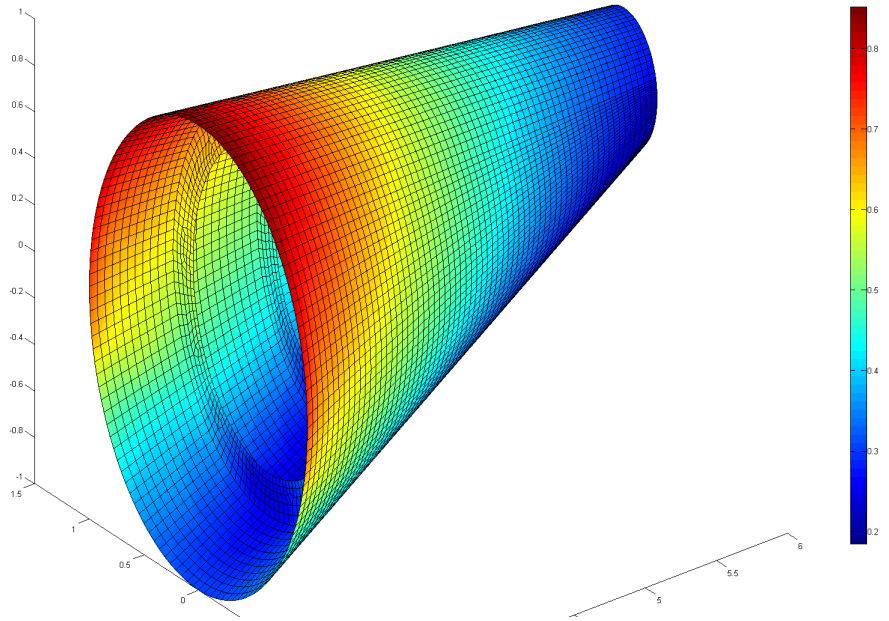

Figure 5.24: Response at 49 Hz before the modification on S19

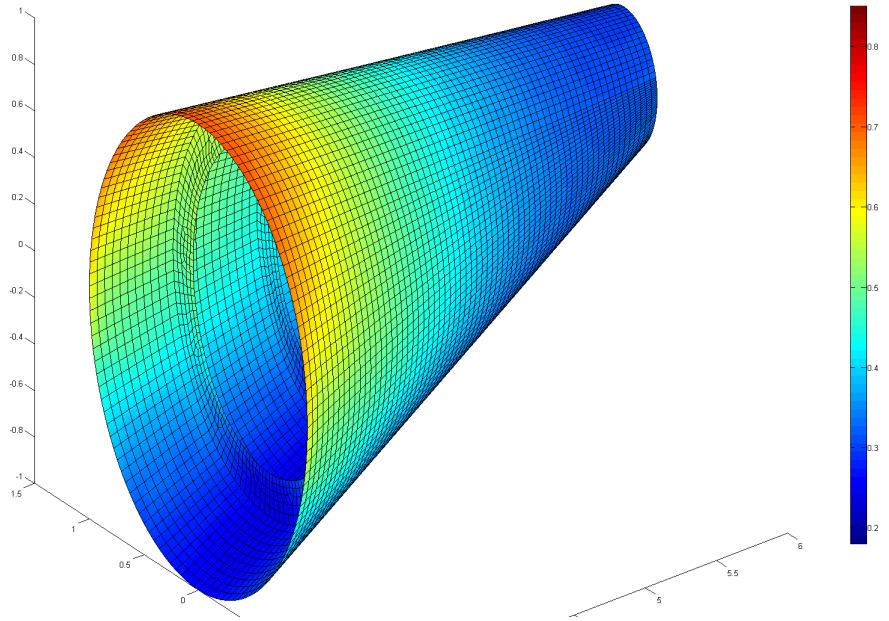

Figure 5.25: Response at 49 Hz after the modification on S19

Optimization for 76 Hz

The sensitive area for 76 Hz is located at the edge of the first reinforcement rib (figure 5.27). Damper elements are therefore attached to some of the nodes around the circle. From figure 5.28 one can see that the response at this area improves significantly. The frequency response curve for the SPL, however, shows only little change around 76 Hz.

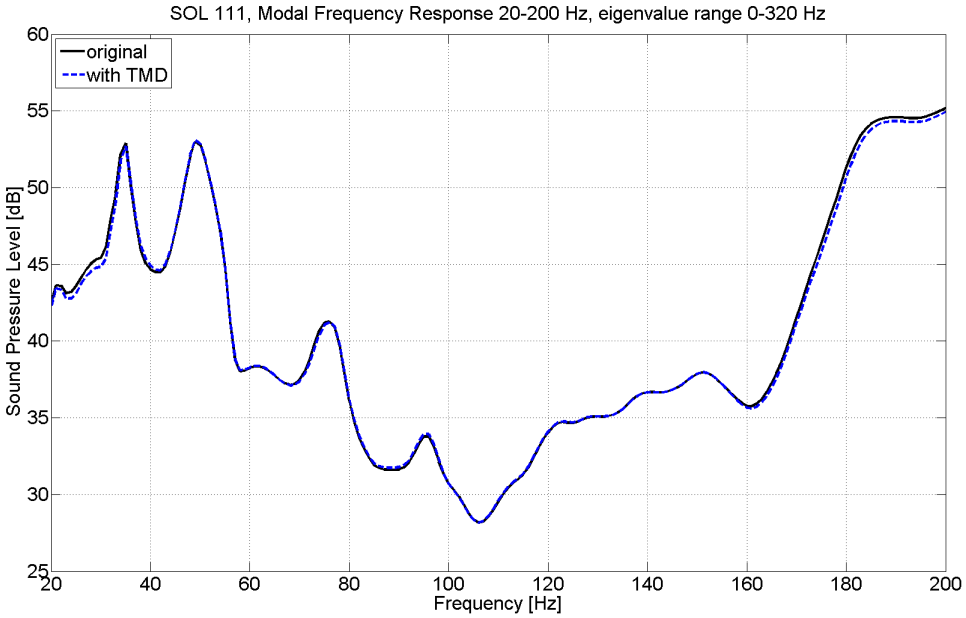

Figure 5.26: SPL comparison between the modified model (for 76 Hz on S19) and the original model

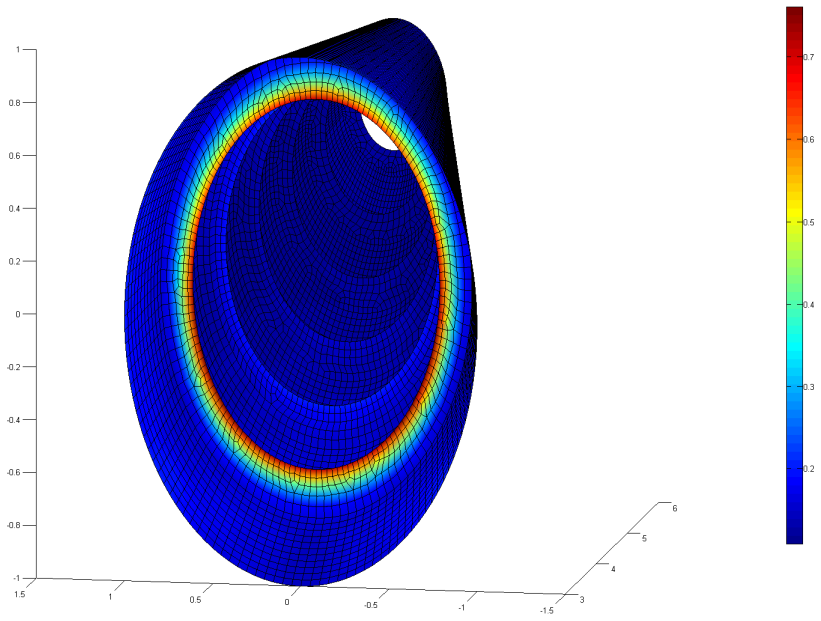

Figure 5.27: Response at 76 Hz before the modification on S19

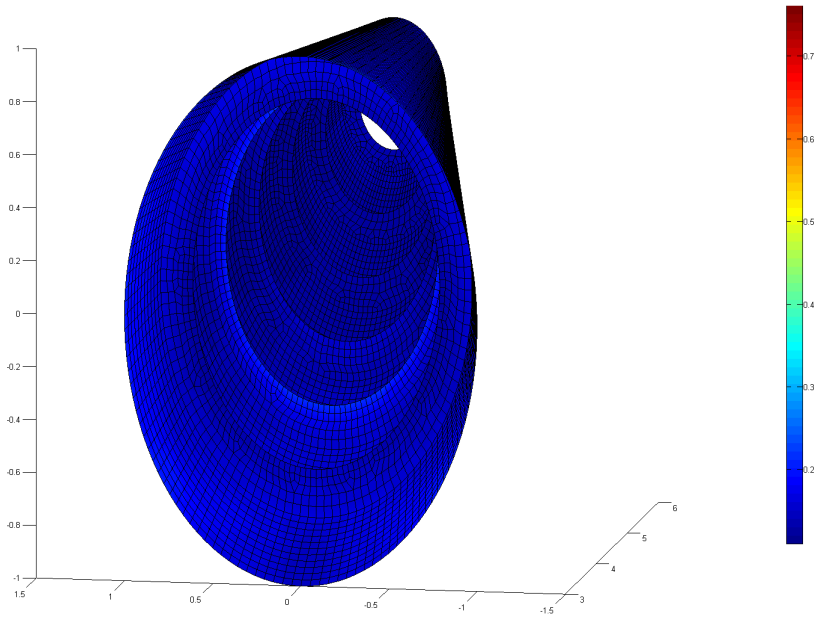

Figure 5.28: Response at 76 Hz after the modification on S19

Optimization for 190 Hz

figure 5.30 shows that, for 190 Hz, the sensitive areas in S19 are located on the first four reinforcement ribs, regularly distributed at 90 degrees. Twelve dampers are used here for each reinforcement rib. The results of this modification are shown in Fig. 5.31. The SPL response is greatly improved for the peak at 190Hz.

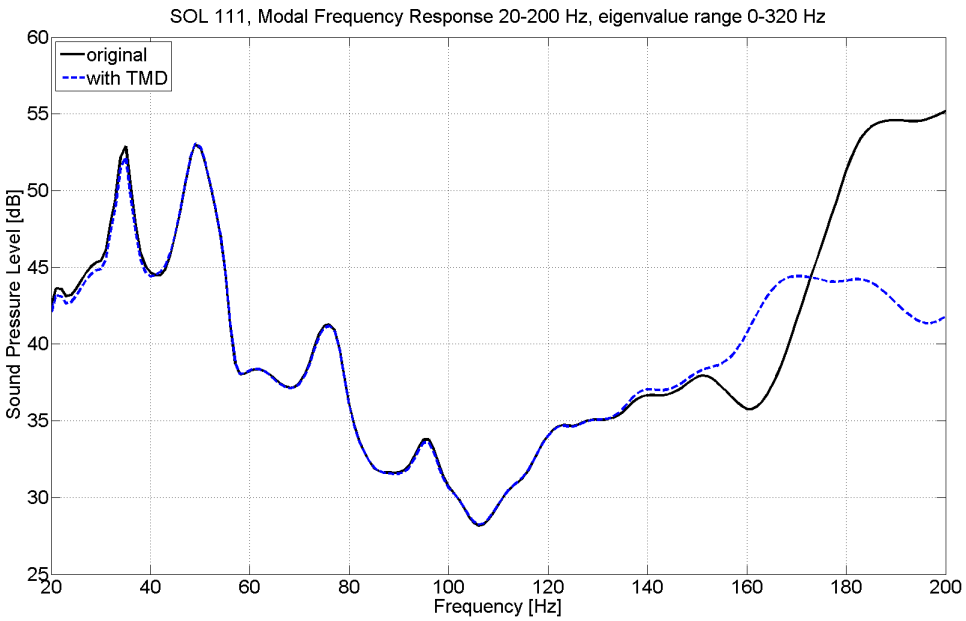

Figure 5.29: SPL comparison between the modified model (for 190 Hz on S19) and the original model

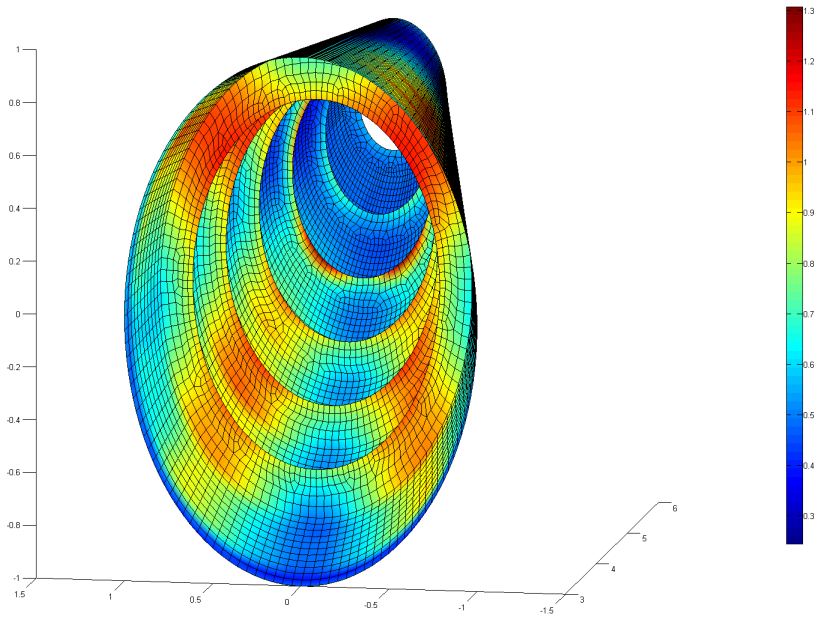

Figure 5.30: Response at 190 Hz before the modification on S19

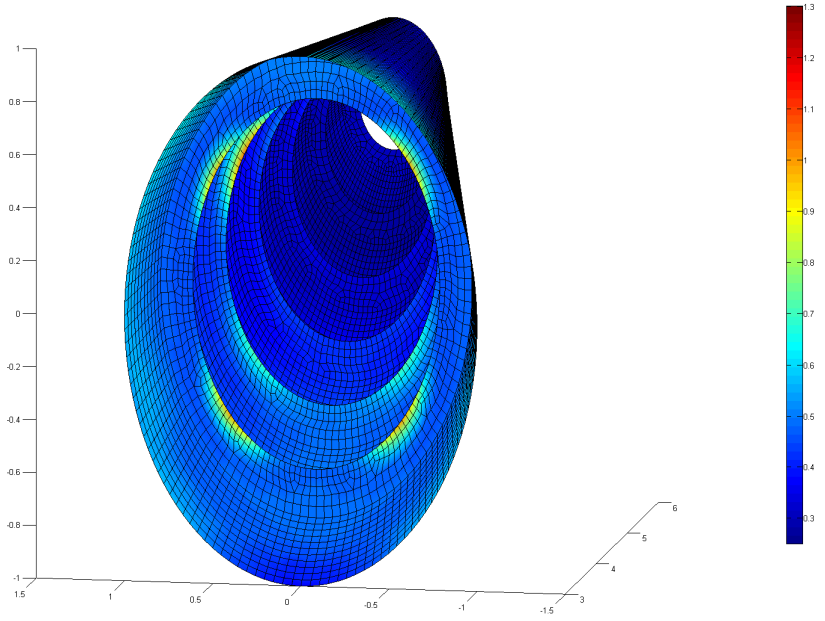

Figure 5.31: Response at 190 Hz after the modification on S19

5.3.3 Optimization on S18

At this time, a brief summary for the results on S19 is necessary before continuing with the optimization of the structure S18. We found that such modifications have a visible effect for some frequencies while not for others. This frequency dependence can be explained by comparing the computed equivalent radiated powers for 76 Hz and 190 Hz.

The results are diagrammed in Fig. 5.32 and 5.33. Different colors represent different regions according to the definition in section 5.2.2. The black curve represents the total ERP. Solid lines are used to indicate the original results, dotted lines are used for the modified results. There is no visible difference for the modifications for 76 Hz, which means the propagation of vibration energy is not influenced by the local modification. The modifications for 190 Hz, on the other hand, have a significant effect on the ERP in the high-frequency range and isolate the sound source well from the receiver.

From both the panel participation factor and from the equivalent radiated power results in previous studies it can be concluded that S18, especially the floor part, has a significant influence on the response at the ear position.

In this section we turned our attention to the optimization on S18. Since the results on the structure are always symmetric, only half of the model is illustrated.

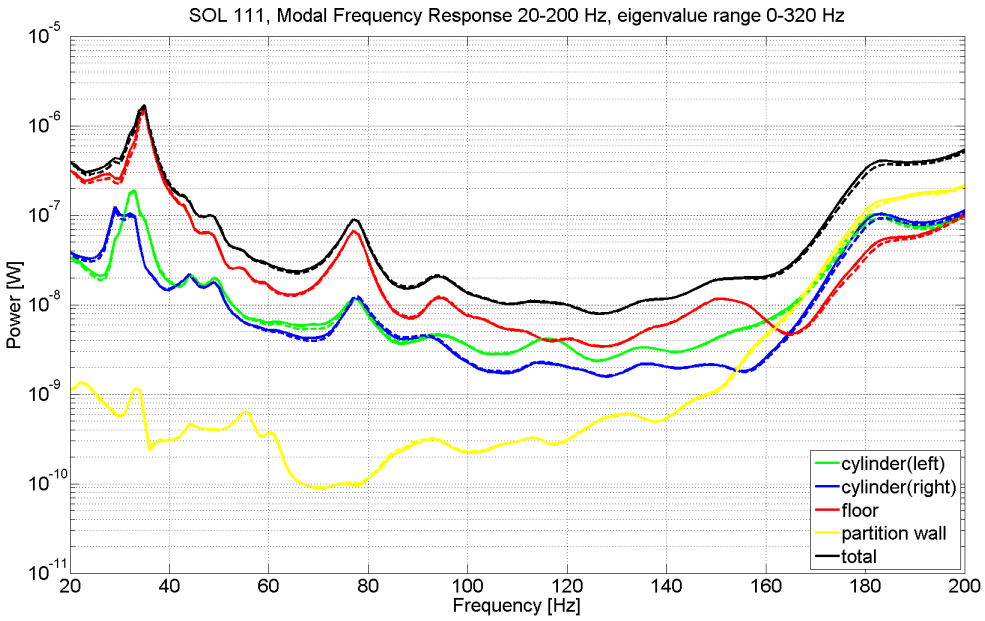

Figure 5.32: ERP comparison between the modified model (for 76 Hz on S19) and the original model

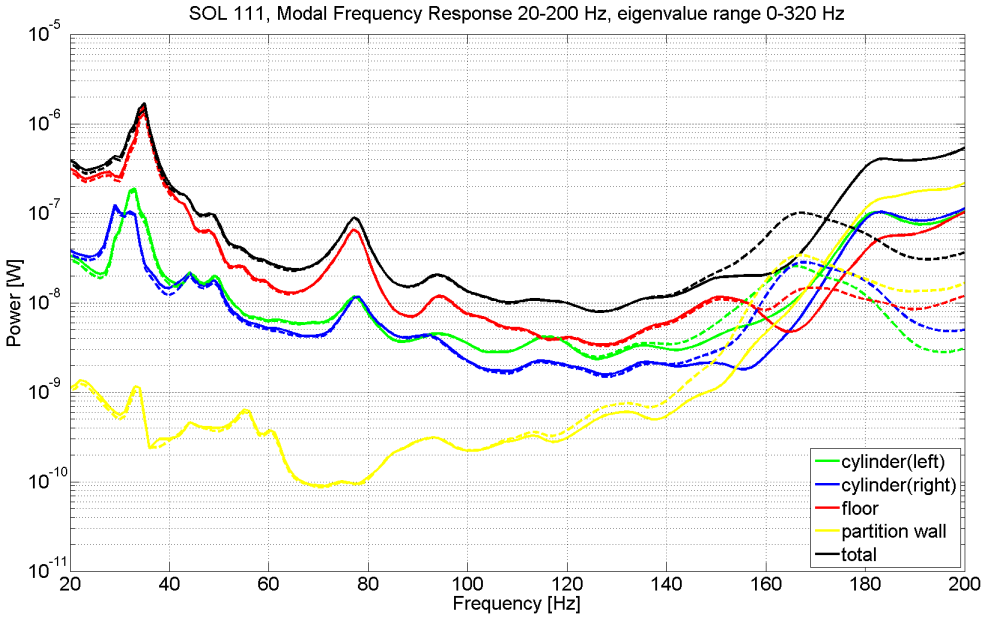

Figure 5.33: ERP comparison between the modified model (for 190 Hz on S19) and the original model

Optimization for 35 Hz

From figure 5.35, one can see that the sensitive area is mainly at the rear of the floor part. By creating tuned mass dampers at the target location the response on the structure is improved (see figure 5.36). In figure 5.34 a significant decrease at frequency 35 Hz can be observed.

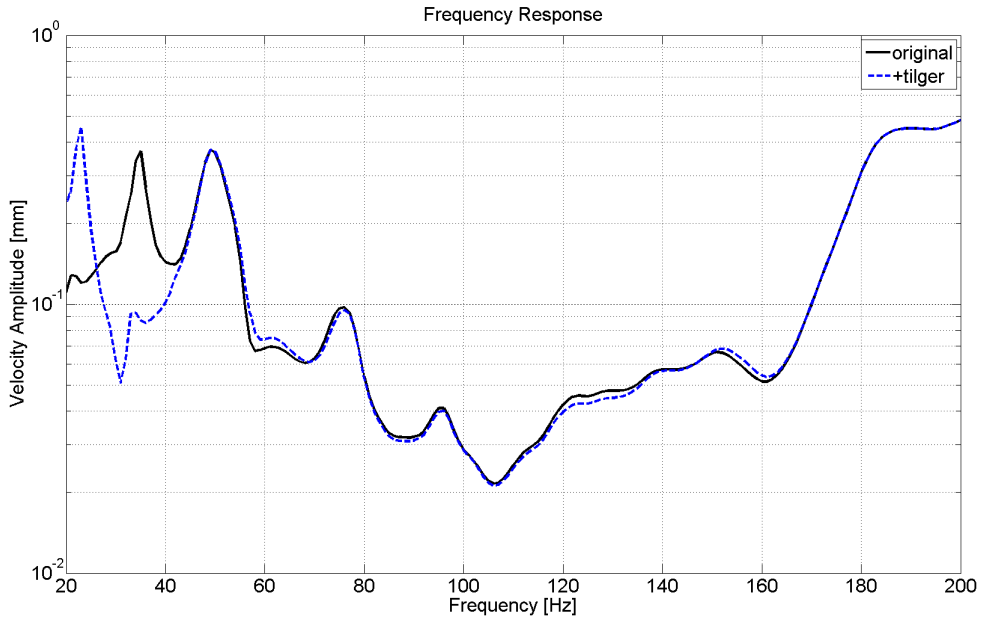

Figure 5.34: SPL comparison between the modified model (for 35 Hz on S18) and the original model

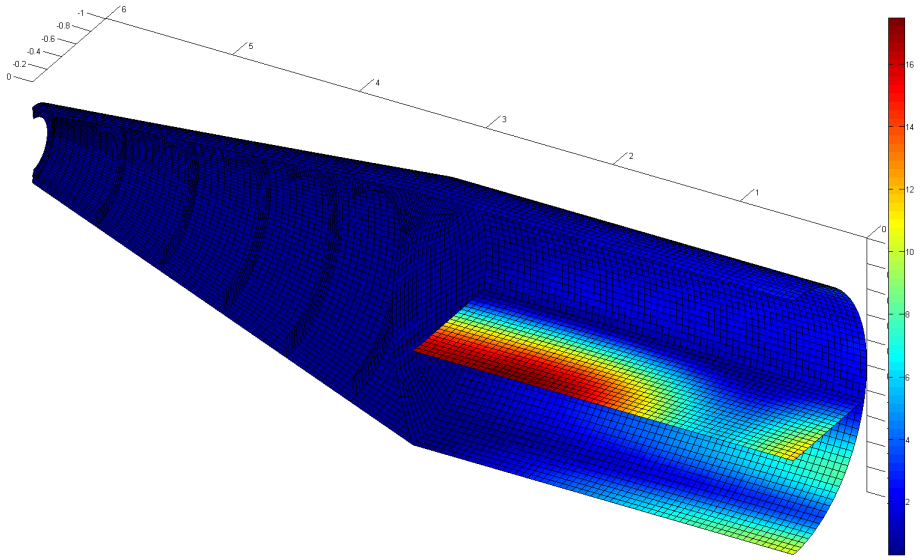

Figure 5.35: Response at 35 Hz before the modification on S19

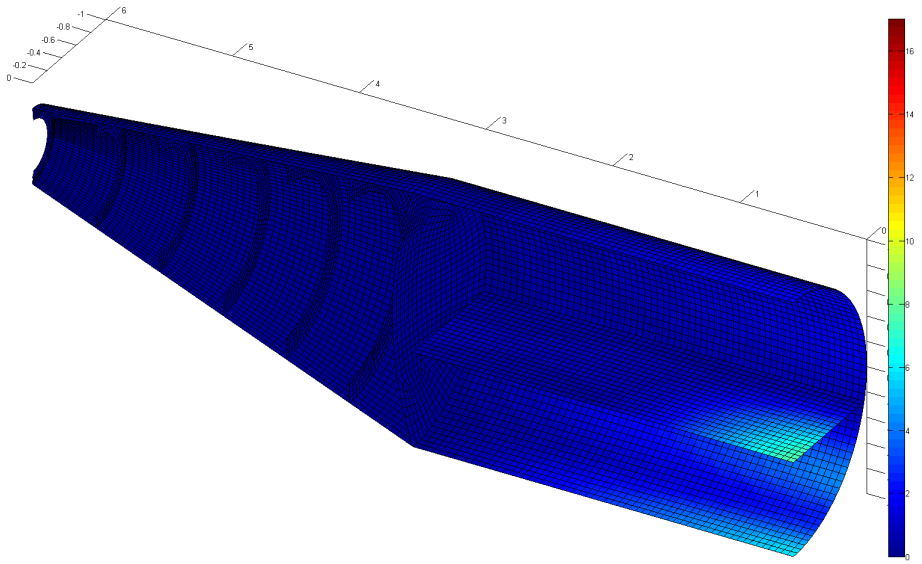

Figure 5.36: Response at 35 Hz after the modification on S19

Optimization for 49 Hz

The sensitive area for 49 Hz is also located at the rear part of the floor. A symmetrical arrangement of dampers is applied to the floor and to some selected node locations on the cylinder exterior. Figure 5.37 shows the effect of the modification, which not only changes the response at 49 Hz but also at lower frequencies.

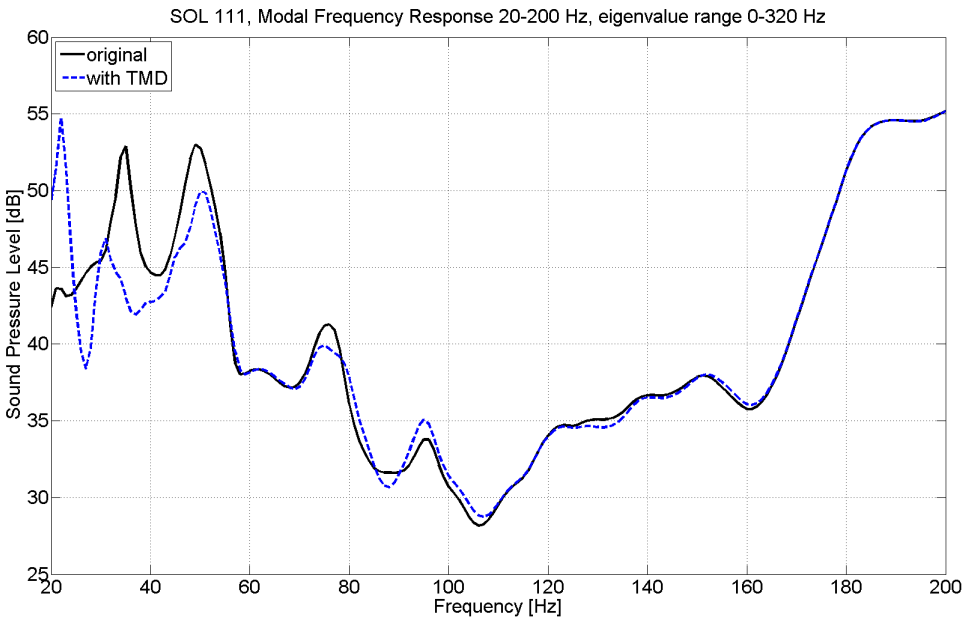

Figure 5.37: SPL comparison between the modified model (for 49 Hz on S18) and the original model

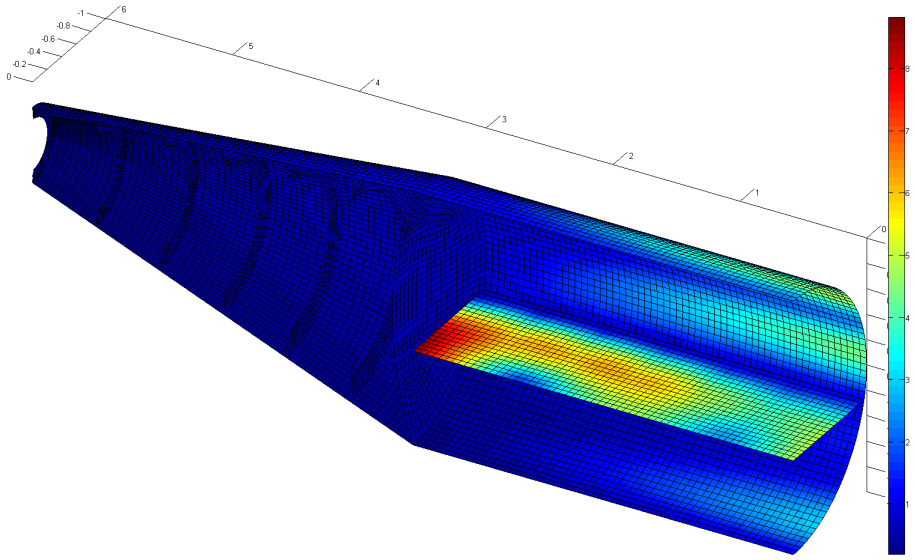

Figure 5.38: Response at 49 Hz before the modification on S19

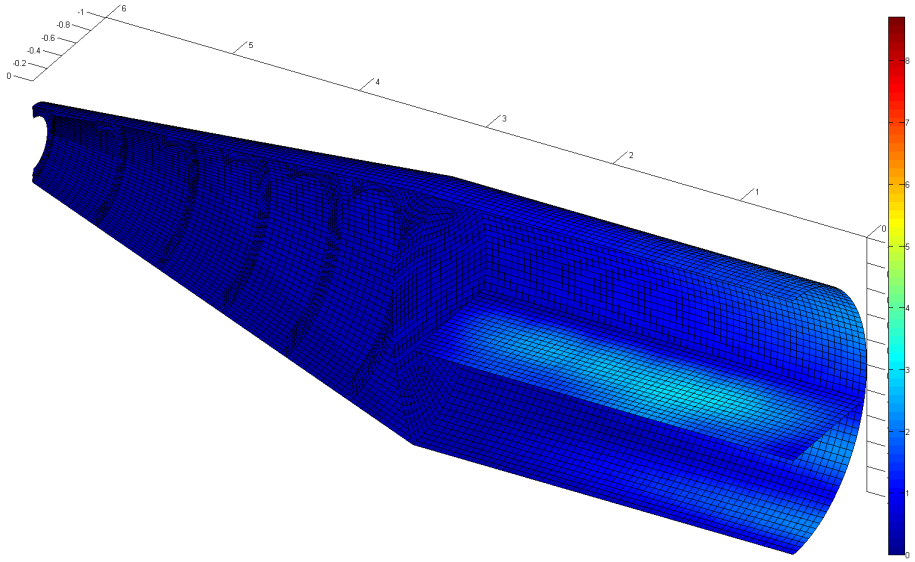

Figure 5.39: Response at 49 Hz after the modification on S19

Optimization for 76 Hz

The sensitive area for 76 Hz is along the x-axis (figure 5.41) of the complete floor. Through a row of dampers the following response in Fig. 5.40 is achieved. The modification intended for 76 Hz causes a decrease of the pressure level in the range from 30 Hz to 100 Hz but unfortunately also produces a new peak at about 23 Hz.

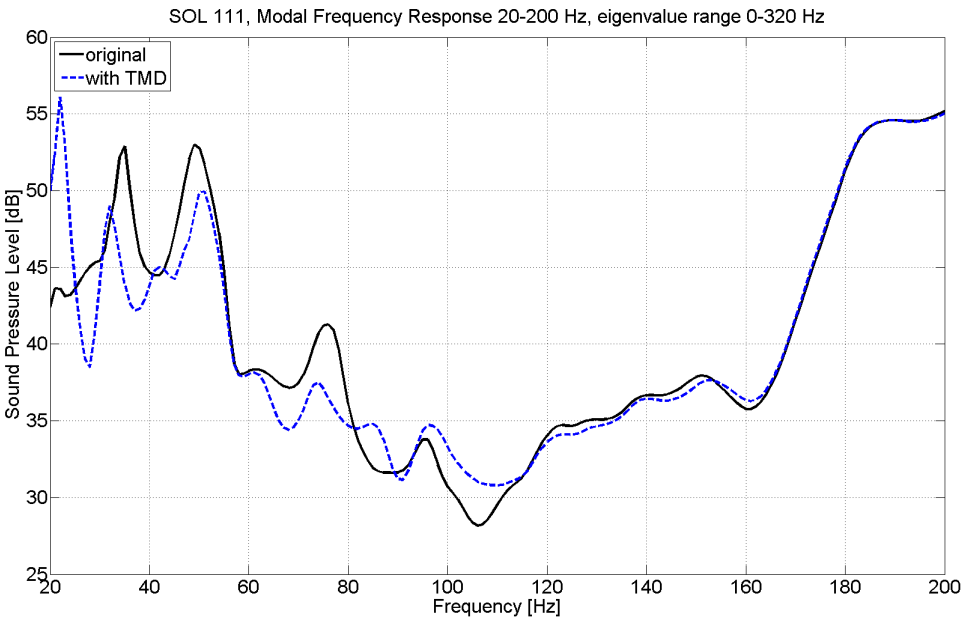

Figure 5.40: SPL comparison between the modified model (for 76 Hz on S18) and the original model

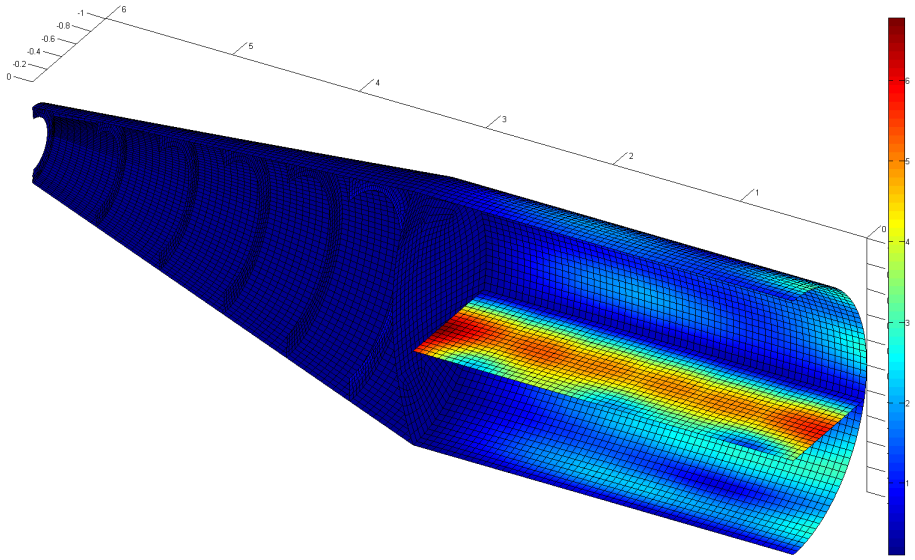

Figure 5.41: Response at 76 Hz before the modification on S19

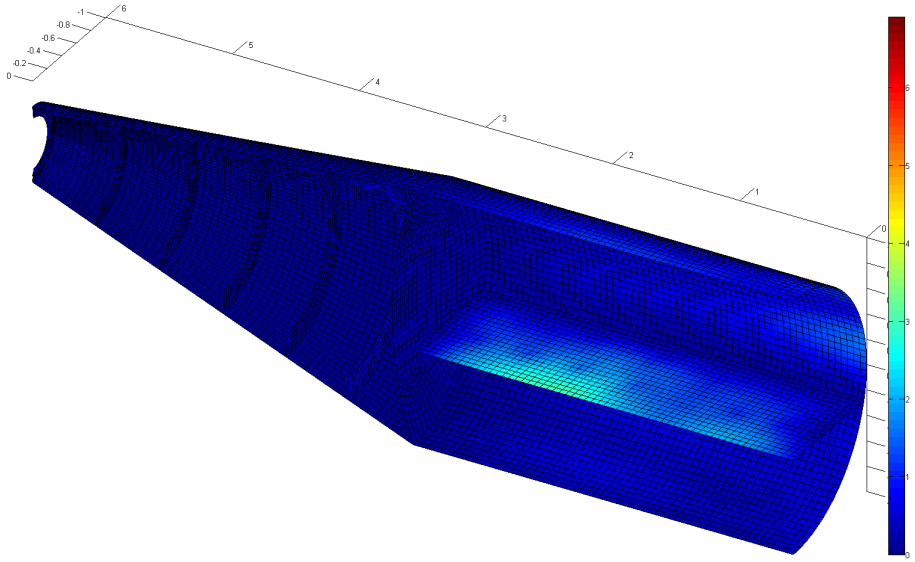

Figure 5.42: Response at 76 Hz after the modification on S19

Optimization for 23 Hz

The new peak pressure level produced at 23 Hz, and caused by the dampers inserted for 76 Hz, needs to be offset. Generally, one should be aware of such side effects and design the modifications with the complete frequency range in mind.
The sensitive areas for 23 Hz are located at the two ends of the floor. The result of inserting dampers is shown in Fig. 5.43 and satisfies the requirement.

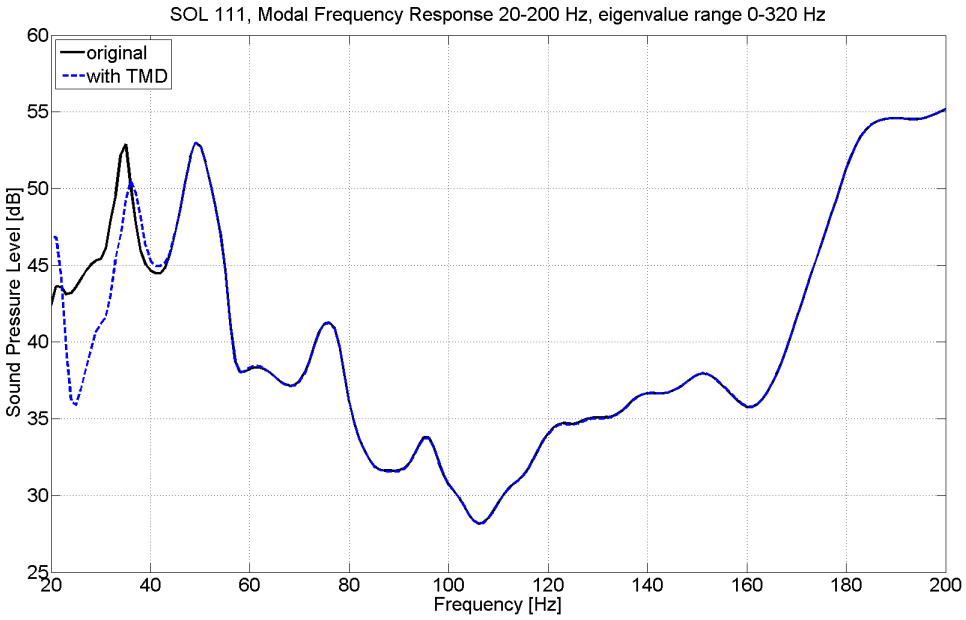

Figure 5.43: SPL comparison between the modified model (for 23 Hz on S18) and the original model

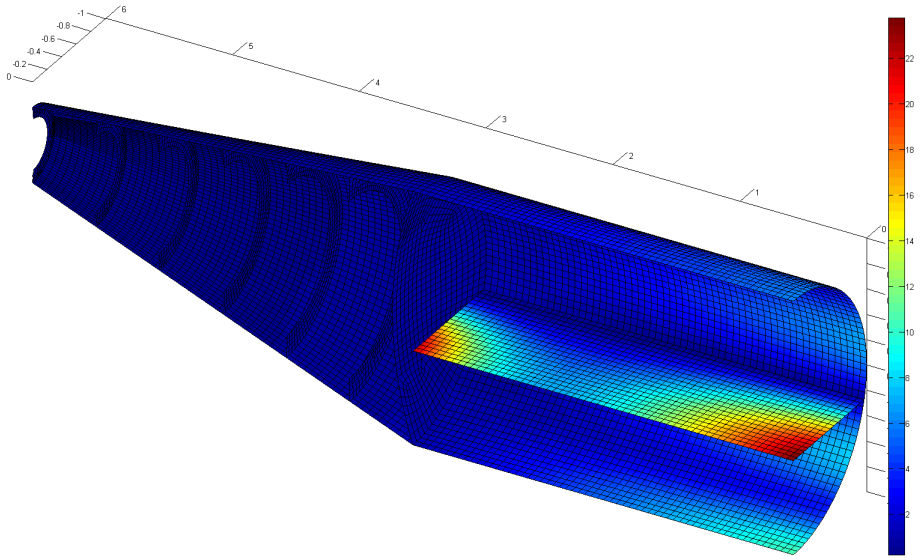

Figure 5.44: Response at 23 Hz before the modification on S19

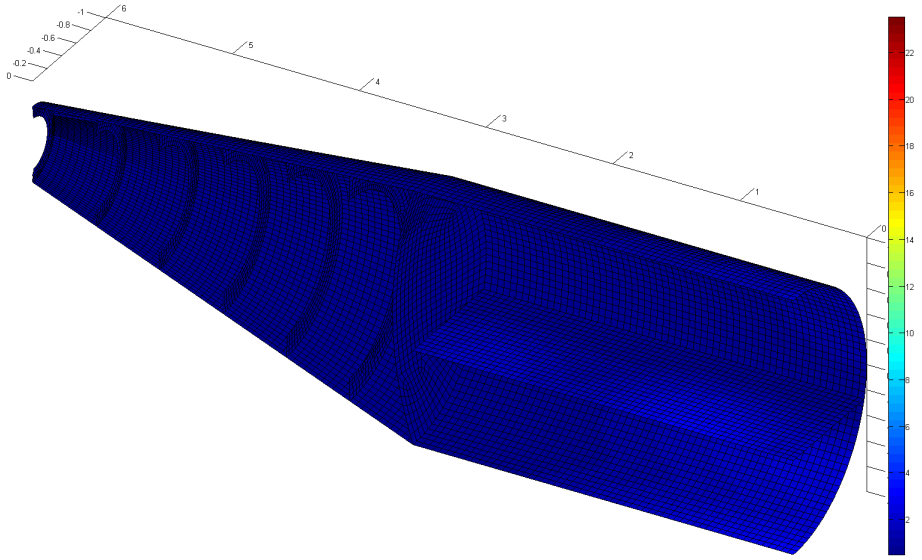

Figure 5.45: Response at 23 Hz after the modification on S19

5.3.4 Combined optimization

Finally, after all the modifications are tested, the results are evaluated to pick the suitable modifications for the combined optimized design. The resulting SPL for the combined optimization is shown in Fig. 5.46.

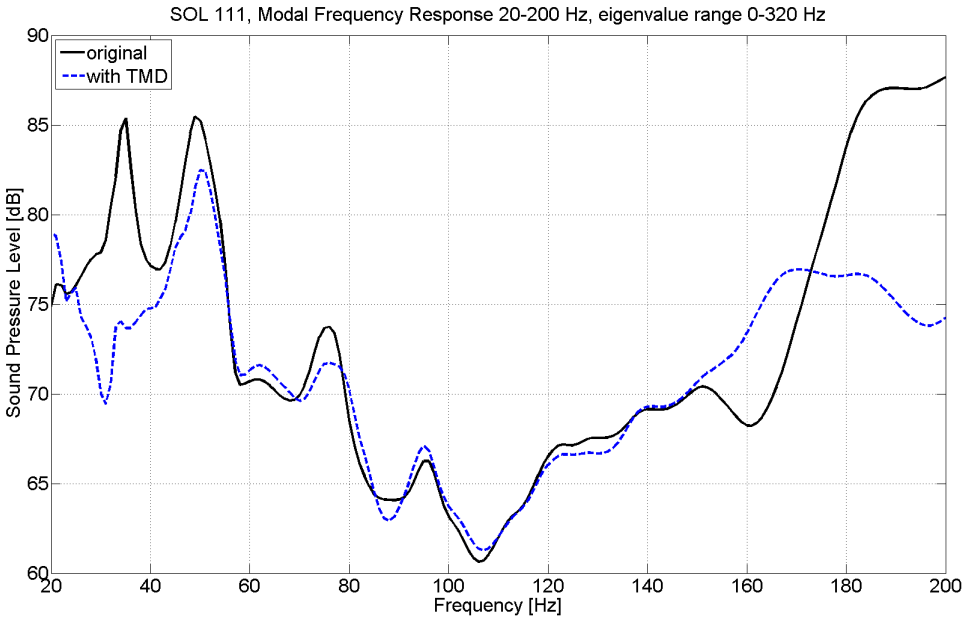

Figure 5.46: SPL comparison between optimized model and original model

The combined damping system results in loudness reductions at the selected frequencies (for the peak pressure levels in the original structure) ranging from 3 dB to 15 dB. Dozens of tuned mass dampers are used for the optimization, with a total weight of 24 kilograms. Of course, the weight of the damper can still be reduced through continuous optimization.

Chapter 6

Conclusion and outlook

As an effective method, reciprocity principle has been widely used to solve structure and fluid problems in many fields. This study extend the application of reciprocity principle to the fluid-structure interaction problems with the finite element method. The reciprocity principle is first applied to the structure optimization of an airplane, then various evaluation procedures are investigated for vibro-acoustic computations. Finally, the feasibility of an optimization procedure for reducing sound pressure levels using the reciprocity principle is proved by this study. The optimization can be performed not only for one single ear position, but also for the whole group of ear positions. One advantage of the usage of the reciprocity principle is, that, one can perform the calculation even if the location of the load is not precisely defined.

To perform the panel participation factor, the cabin part of the fuselage is subdivided into one floor region, one wall region and two skin regions. The computation results show: In the low frequency range, the floor region plays the leading role while the partition wall is completely irrelevant. For high frequencies, on the other hand, all the structure parts are more or less significant.

After the weak points of the structure are found and modified by inserting tuned mass dampers, various methods such as determining the equivalent radiated power can be applied to evaluate the effect of the optimization. In Nastran, ERP provides an approximate value for the acoustic power radiated from the structure. And compare to the ACPOWER command, the computing time can be saved to a large extent by using ERP.

There is still room for improvement and further optimization. For example the number of tuned mass damper can be reduced through continuous optimization. Besides, a symmetric load can be employed so that some pressure peaks will disappear and the result is closer to reality, which also means less weight used for dampers.

Bibliography

[1] F. Ihlenburg, *Computational Acoustics*, lecture notes (2011)

[2] F. Ihlenburg, *Finite Element Analysis of Acoustic Scattering*, Springer-Verlag (1998)

[3] K.J. Bathe, *Finite Element Procedures*, Prentice Hall (1996)

[4] F. Ihlenburg, *Sound in Vibrating Cabins: Physical Effects, Mathematical Description, Computational Simulation with FEM*2006

[5] Earl G. Williams, *Fourier Acoustics: Sound Radiation and Nearfield Acoustical Holography*, Academic Press (1999)

[6] MSC.Software Corporation, Dynamic Analysis User's Guide (2011)

[7] MSC.Software Corporation, Nastran Quick Reference Guide (2010)

[8] F. J. Fahy, *Some Applications of the Reciprocity Principle in Experimental Vibroacoustics*, 2002

[9] L. M. Lyamshev, *A Question in Connection with the Principle of Reciprocity in Acoustics*, 1959

[10] MSC.Software Corporation, Nastran Release Guide (2010)

[11] Wu Guangqiang, Sheng Yun, Fang Yuan, *Coupled Acoustic-structural Finite Element Analysis of Vehicle Interior Noise Based on Acoustic Sensitivity*, 2009

[12] Wang Jun, Ning Wei, Zhang Jinghui, *Numerical Simulation of Reverberant Acoustic Field Adopting Reciprocity Theorem*, 2010

[13] K. Wiechmann, J. Hiller, *Evaluation and Visualization of Equivalent Radiated Power*, 2011

[14] http://en.wikipedia.org/wiki/Helmholtz_equation

[15] http://www.esm-gmbh.de/EN/Products/Tuned_mass_dampers

[16] http://www.airliners.de/management/marketing/lufthansa-zeigt-neue-europa-kabine/22909

[17] http://www.pmi.lv/soft/stirel/index.htm

Appendix A

Nastran input file for SPL Response

```
$ MODAL FREQUENCY RESPONSE
   SOL 111
CEND
$
  TITLE= FLUID-STRUCTURE-RESPONSE
  SUBTITLE = Force Excitation structure 1N, Response Fluid, 20-200Hz
  LABEL = Modal 0-320HZ
  ECHO = NONE
$
$ Measuring points for 42 ear positions
SET 1 = 747064,747148,749022,750134,750218,752246,753066,753150,755470,
755998,756082,757550,757634,758694,759078,760482,760566,762302,763304,
763421,765478,767316,767400,769114,770210,770294,772194,772982,773066,
775274,775754,775838,777306,777390,778354,778674,780078,780162,781754,
782740,782857,784794
$ fluid response output
DISPLACEMENT(PLOT,SORT1,REAL,PUNCH)=1
$
  METHOD(STRUCT) = 50
  METHOD(FLUID)  = 51
  FREQ   = 200
  DLOAD = 2000
$
BEGIN BULK
$
$ Fluid and Structure meshes
include 'FEM_all_coupled.bdf'
$ Absorbing boundary meshes
include 'CAABSF.bdf'
$
$1......2.......3.......4.......5.......6.......7.......8.......9.......
PARAM   AUTOSPC YES
```

```
PARAM   POST    -1
$
$ ABSORBING BOUNDARY CONDITIONS
$1......2.......3.......4.......5.......6.......7.......8.......9.......
PAABSF  10                                      210.8           210.8
$ DYNAMIC LOADING ON STRUCTURE
$1......2.......3.......4.......5.......6.......7.......8.......9.......
DLOAD   2000    1.      1.      2001
RLOAD1  2001    2001                    1111
$               Dynamic load at Grid 8373 (mechanical source) 1N
DAREA   2001    8373    3       1.0
$ Referenced Dynamic Load Tables
$ Constant Load Table
TABLED1  1111
         0.     1.      1000.   1.       ENDT
$ METHOD CARD EIGENVALUE
$1......2.......3.......4.......5.......6.......7.......8.......9.......
$ Structure frequency range of interest
EIGRL   50      -1.e-1  320.
$ Fluid frequency range of interest
EIGRL   51      -1.e-1  320.
$
$ Frequency range
FREQ1   200     20.0    1.0     180
$1......2.......3.......4.......5.......6.......7.......8.......9.......
$ Damping coefficient for both structure and fluid
PARAM   G       0.06
PARAM   GFL     0.06
$
$ FLUID STRUCTURE PARAMETER
$1......2.......3.......4.......5.......6.......7.......8.......9.......
ACMODL  DIFF                                    BW
$
ENDDATA
```

Appendix B

Nastran input file for reciprocal calculation

```
$ MODAL FREQUENCY RESPONSE
   SOL 111
CEND
$
  TITLE= FLUID-STRUCTURE-RESPONSE
  LABEL = Modal 0-320HZ
  ECHO = NONE
$ Measuring points for all structure nodes
SET 1 = 4920 THRU 4935,5076,5111,5122,5133,5144,5155,5166,5177,5188,
5199,5210,5221,5228,5237,5246,5257,5268,5281,5293,5309,5481 THRU 5495,
.................................................................
.................................................................
33319 THRU 33329,33331 THRU 33341,36729 THRU 37419,37540 THRU 38151,
38272 THRU 38775,38896 THRU 39346,39467 THRU 39802,39923 THRU 40247,
40248
$
$ Structure output
VELOCITY(PUNCH,SORT1,REAL)=1
METHOD(STRUCT) = 50
METHOD(FLUID)  = 51
FREQ   = 200
$
$ Subcase for all ear position
$
SUBCASE 1
DLOAD = 1
SUBCASE 2
DLOAD = 2
.........
```

```
.........
.........
SUBCASE 41
DLOAD = 41
SUBCASE 42
DLOAD = 42
$
BEGIN BULK
$
$ Fluid and Structure meshes
include 'FEM_all_coupled.bdf'
$ Absorbing boundary meshes
include 'CAABSF.bdf'
$
$1......2.......3.......4.......5.......6.......7.......8.......9.......
PARAM   AUTOSPC YES
PARAM   POST    -1
$
$ Absorbing boundary conditions
$1......2.......3.......4.......5.......6.......7.......8.......9.......
PAABSF  10                                      210.8           210.8
$
$ Damping coefficient for both structure and fluid
$1......2.......3.......4.......5.......6.......7.......8.......9.......
PARAM   G       0.06
PARAM   GFL     0.06
$
$ Frequency range
$1......2.......3.......4.......5.......6.......7.......8.......9.......
FREQ    200     190.0
$
$ Fluid stucture parameter
$1......2.......3.......4.......5.......6.......7.......8.......9.......
ACMODL  DIFF                                    BW
$
$ Structure frequency range of interest
EIGRL   50      -1.e-1  320.
$ Fluid frequency range of interest
EIGRL   51      -1.e-1  320.
$
$ Acoustic source
$
$1......2.......3.......4.......5.......6.......7.......8.......9.......
ACSRCE  1       1001                    1111    1.24    35836.
SLOAD   1001    767316  1.0
```

```
$1......2.......3.......4.......5.......6.......7.......8.......9.......
ACSRCE  2       1002                    1111    1.24    35836.
SLOAD   1002    767400  1.0
                 ..............................
                 ..............................
                 ..............................
$1......2.......3.......4.......5.......6.......7.......8.......9.......
ACSRCE  41      1041                    1111    1.24    35836.
SLOAD   1041    763304  1.0
$1......2.......3.......4.......5.......6.......7.......8.......9.......
ACSRCE  42      1042                    1111    1.24    35836.
SLOAD   1042    765478  1.0
$
$ quadratic function
$1......2.......3.......4.......5.......6.......7.......8.......9.......
$
TABLED4 1111    0.0     1.0     0.0     1.E6
        0.0     0.0     0.0115  0.0     ENDT
ENDDATA
```

Appendix C

Matlab graphing programm

```
clear all; close all; clc;
freq=[];

%% read file
fname='fsi_excit_fluid_plot';
fpch=[fname,'.pch'];
display(['Processing file: ',fpch]);
fid=fopen(fpch,'r');
while 1
    l=fgetl(fid);
    if strncmp(l,'$FREQ',5)
        freq(end+1)=str2double(l(13:30));
    end
    if l==-1;break;end
end
number_of_freqs=length(freq);
% read pch data
frewind(fid);
c=textscan(fid,'%s','commentStyle','$');
% process pch data
entries_per_mp=21;
number_of_mp=length(c{1})/number_of_freqs/entries_per_mp;
cx=reshape(c{1},entries_per_mp,number_of_mp,number_of_freqs);
% Displacement Amplitude: 3:5 = real part, 13:15 = imag part
uu=str2double(squeeze(cx([3:5,13:15],:,:)));
% absolute value of displacement or pressure
abs_u(:,:)=sqrt(dot(uu,uu,1));
clf;

frewind(fid);
ID_C=zeros(number_of_mp,2);
i=1;
```

```
while i<=number_of_mp
        l=fgetl(fid);
    if strncmp(l,'    ',4)
        ID_C(i,1)=sscanf(l(1:12),'%d',1);
        ID_C(i,2)=sum(abs_u(i,:));
        i=i+1;
    end
    if l==-1;break;end
end
fclose(fid);

%% read element
file='S18_S19.bdf';
fid=fopen(file,'r');
cqc=0;
disp(['=> Reading bulk data from ', file]);
clear block_0;
[block_0]=fread(fid,'*char').';    % read 100 000 000 characters into block_0
CQUADc=strfind(block_0,'CQUAD4');
CQUAD_size=length(CQUADc);
CQUAD=zeros(CQUAD_size,5);

for m = 1:CQUAD_size
        index = CQUADc(m);
        cqc=cqc+1;
        CQUAD(cqc,1) =sscanf(block_0(index+ 8:index+15),'%d',1);
        CQUAD(cqc,2) =sscanf(block_0(index+24:index+31),'%d',1);
        CQUAD(cqc,3) =sscanf(block_0(index+32:index+39),'%d',1);
        CQUAD(cqc,4) =sscanf(block_0(index+40:index+47),'%d',1);
        CQUAD(cqc,5) =sscanf(block_0(index+48:index+55),'%d',1);
end
fclose(fid);

%% read nodes
[node,pos]=readGEOM12('FEM_all_coupled.bdf');

%% make plot
ID=zeros(1,4);
X=zeros(1,4);
Y=zeros(1,4);
Z=zeros(1,4);
C=zeros(1,4);

hold on;
%for i=1:4000
```

```
for i=1:CQUAD_size
    for j=1:4
        ID(j)=CQUAD(i,j+1);
        k=1;
        while 1
        if ID(j)==node(k);
            X(j)=pos(k,1);
            Y(j)=pos(k,2);
            Z(j)=pos(k,3);
            break;
        end
        k=k+1;
        end
        m=1;
        while 1
            if m>10960  %max point
                break;
            end

        if ID(j)==ID_C(m,1);
            C(j)=ID_C(m,2);
            break;
        end
        m=m+1;
        end
    end
    if max(Y)<0.01
    fill3(X,Y,Z,C)
    end
end
view(30,150)
axis equal;
colorbar;
caxis([0.5 23.5]);
%view(3);
print('-dmeta',[fname,'.emf'])
```